June 1987

DCIEM No. 87-RR-19

DIGITAL PROCESSING OF DOPPLER ULTRASONIC SIGNALS FOR INTRAVASCULAR BUBBLES

B.C. Eatock

D.M.C. Sweeney

Defence and Civil Institute of Environmental Medicine
1133 Sheppard Ave. W., P.O. Box 2000
Downsview, Ontario, Canada M3M 3B9

DEPARTMENT OF NATIONAL DEFENCE - CANADA

Table of Contents

Abstract 1

1. Introduction 2

    1.1 Object 2

    1.3 Literature Review 2

    1.2 History of DCIEM Developments 4

2. Characteristics of Doppler Ultrasonic Signals 5

    2.1 Temporal Characteristics 5

    2.2 Averaged Spectral Characteristics 6

    2.3 Short-Time Spectra 7

3. Description of the Algorithm 9

4. Tests of the Algorithm 11

    4.1 Methods 11

    4.2 Results 12

        4.2.1. Results for initial parameter set 12

        4.2.2. Effect of filter 14

        4.2.3. Effect of threshold 15

        4.2.4. Effect of α 15

        4.2.5. Effect of β 15

        4.2.6. Effect of sampling rate 15

        4.2.7. Effect of buffer size 16

5. Discussion 17

6. Recommendations 18

Acknowledgements 18

References 18

Appendix A. The K-M Code for Describing Doppler Ultrasonic Bubble Data 21

    Parameters 21

    Frequency - both cases 21

    Percentage - rest case 21

    Duration - movement case 22

    Amplitude - both cases 22

Figure Captions 22

Figures 27

ABSTRACT

This report describes progress made in the development of a system for the automatic detection of bubbles by digitally processing Doppler ultrasonic signals. The system was developed primarily because of the need for an objective means of counting bubbles in the blood of divers, aviators, or other individuals who have been subjected to a reduction in ambient pressure. The number of bubbles is thought to indicate the stress felt by an individual as a result of the decompression. The characteristics of the signals are described, and the theory underlying the development of the algorithm is developed. The results of tests of the algorithm on various signals are presented. The algorithm is successful at detecting the presence of bubbles when they are moderately frequent, but does not distinguish infrequent bubbles from normal cardiac signals, and fails to distinguish bubbles when they are extremely numerous. To deal with the latter case, pattern matching should be used.

1. Introduction

1.1. Object

Doppler ultrasonic bubble detection is now used in several laboratories, as a means of evaluating the decompression stress associated with diving (1-8). Dives producing many intravascular bubbles in most divers are considered unsafe. The technique, as it is used however, is subjective and qualitative. The observer listens to the Doppler-shifted component of the scattered ultrasound. The observer attempts, first to identify bubble signals, and then to classify them according to a grading scheme, such as that of Spencer (1) or Kisman and Masurel (9-12). Appendix A gives an explantion of the *K-M Method*. The Doppler technique is dependent on the expertise and the vigilance of the listener. Furthermore, it is time-consuming, tedious, and labour-intensive.

This report describes progress made in the development of a system for the automatic detection of bubbles by digitally processing Doppler ultrasonic signals. The object of processing the Doppler signal is to render the technique quantitative, more reliable, and less demanding. The system is based on an algorithm developed by Kisman (13).

The Doppler ultrasonic signal consists of signals scattered by all moving surfaces in the field of view of the ultrasonic transducers, including blood corpuscles, the walls of blood vessels, and, if present, bubbles. The ultrasonic instrument demodulates the received ultrasonic signal to extract the Doppler-shifted component. The resulting signal falls in the audio region, and is usually interpreted by human observers. Several investigators have attempted to characterize the signals and to develop sytems for automatically detecting and counting them.

1.2. Literature Review

Smith and Spencer (14) showed spectrograms of Doppler ultrasonic signals from probes implanted in sheep. The frequencies of the bubble signals ranged from 500 to 2000 Hz.

Nishi and Livingstone (15) observed changes in the shape of the Doppler spectrum during decompression even in the absence of distinguishable bubbles. They hypothesized that these changes might result from aggregation of platelets or erythrocytes.

Guillerm *et al.* (16) briefly described the use of a filter and integrator for processing Doppler signals obtained from probes implanted in animals. According to Guillerm and Masurel (17) most of the background signal could be eliminated by using a high-pass filter with a cut-off frequency of 800 Hz. Monjaret, Guillerm, and Masurel (18), however, said that this frequency should be varied between 280 and 1800 Hz, depending on the vessel being monitored. Following the filter, these authors used a threshold detector to reduce the background signal scattered by the constituents of the blood. The resulting bubble signal was conjectured to be roughly proportional to the radius of the bubbles. It was then amplified using a third power characteristic to produce a signal approximately proportional to the volume of the bubbles (19). This signal was then integrated, and the integrator was continually reset at a pre-determined interval. The output of the integrator was displayed on a chart. This system has been used extensively and successfully with animals (20), but not with the more complicated signal obtained from human subjects.

Belcher, Ehrenberg, and Lytle (21) described an adaptive algorithm for detecting bubbles in Doppler ultrasonic signals from the pulmonary artery in humans. The algorithm was an enhancement to a non-adaptive system, first developed to count bubbles in Doppler signals from implanted probes used with animals. The first version of this system was not adaptive, and consisted of a bank of 12 four-pole Butterworth, analogue filters having Q's (the ratio of centre frequency to bandwidth, a measure of selectivity) ranging from 6 to 8. The filters were followed by envelope detectors and threshold detectors. If the level at the output of any filter exceeded the threshold set for that frequency, a counter was incremented. In tests of this system with human subjects, Belcher et al. found that, when the threshold was set to achieve an acceptably low false-alarm rate, the detection rate was too low. Their system was improved by subtracting the average of the levels at the output of all filters from the level at each filter. Broad-band increases in level would therefore tend to have a smaller effect, while narrow-band signals would be emphasized.

Belcher et al. stated that significant additional improvements could be obtained by making the algorithm adaptive. In that case, an estimate of the background signal level for each filter would be subtracted from its output. This level would change gradually, to reflect the overall changes in the signal. The estimate would be obtained by sampling two disjoint filters, (e.g., for the fifth filter, samples would be taken from the third and seventh filters). Each disjoint filter would be sampled five times, twice preceding, one concurrent with, and two following the current sample.

Belcher (22) described the implementation of this algorithm, and also discussed the properties of bubble signals leading to its choice. In his model, the bubble signals have a narrow bandwidth, with centre frequency dependent on their speed of passage. They have envelopes dependent on position in the ultrasonic beam, and the duration of the envelope is inversely proportional to their velocity. Faster bubbles have a shorter duration and a wider bandwidth. Belcher's algorithm was designed to exploit these properties.

In the final version of Belcher's system, the number of filters was increased to 16, and the number of samples from disjoint filters was reduced to two from each of two filters. In experiments with animals, the system produced counts indicative of the number of bubbles thought to be present in the blood.

Kisman (23) considered the problem of processing Doppler ultrasonic signals to detect bubbles. He suggested the use of spectrum analysis using records of duration slightly longer than that of a typical bubble transient, estimated to be about 10 ms. He also pointed out some of the salient features of the signals. The background signal is nonstationary; that is, the statistics of the signal change with time. The bubble signals are usually transient. The appropriate functions for representing the spectral characteristics of such signals are energy density functions (23) (24), (p.367). Kisman recommended processing the Doppler ultrasonic signals using Fourier analysis, based on studies with a Fourier analyser of tape-recorded signals from probes implanted in rabbits and miniature swine.

Kisman (13) described an algorithm for processing the Doppler ultrasonic signal to detect and count bubbles. Autospectra (or power spectra) (25), (p. 50), are calculated for consecutive blocks of data. Each autospectrum is then compared with its predecessor and successor by subtraction. The resulting difference or *transient* spectra are compared against a threshold. If the threshold is exceeded for both forward and backward differences, then a transient is deemed to have occurred. Such transients are interpreted as bubbles. In Kisman's model, the occurrence of a bubble is a transient event, and the algorithm developed

by him and D.M.C. Sweeney uses the transient nature of the bubbles to distinguish them from other scatterers contributing to the Doppler signal. The principle of the technique was that different events in the Doppler signal have widely differing characteristic durations. The algorithm was tuned to the duration of the bubble events. Kisman advocated using the number of bubbles so detected as an objective indicator of decompression stress.

1.3. History of DCIEM Developments

The original system assembled to calculate Kisman's algorithm (13) consisted of a PDP 11/10* minicomputer with diskettes, a MAP 200† array processor, an analogue tape recorder, a strip-chart recorder, and analogue-to-digital converters (ADC) (Figure 1).

Although it was intended that this system should run in real-time, it was unable to do so. The recorded signals had to be played back at a speed 32 times slower than real time. Also, the system proved to be unreliable. (It "crashed" frequently.) Despite these difficulties, Kisman claimed to have obtained good agreement between results he obtained using his signal processor and the results obtained independently by an expert who graded the signals aurally**.

Steps were taken to speed up the algorithm, by improving both hardware (Figure 2) and software. The MAP 200† array processor was upgraded to a MAP 300†. In addition, an analogue data acquisition module (ADAM) was purchased for the MAP, so that data could go directly to the MAP, by-passing the host computer. The PDP 11/10 was exchanged for a PDP 11/40*, with more memory, including a cache memory, and a floating point instruction set, but no floating point processor.

More recent versions of the system software were purchased. An *automatic gain control* was added to the program, but this exacted a significant processing penalty. Attempts were made to streamline the program. The amount of processing done by the Array Processor was reduced because of a bottleneck resulting from too many calls to the array processor. All calculations done in the host minicomputer used integer arithmetic, and the program was rewritten in *C*, claimed to be a more efficient language than FORTRAN (26).

The predicted improvements in speed did not occur, however. The speed was only doubled, and this could be attributed to changes in hardware.

Efforts were therefore made to reduce the size of the programs. Comparison tests using recorded data from humans showed that some of the code was redundant. By removing this code, and using the MAP's ADAM, a factor of four improvement in speed in the Fortran version was obtained. The program was then able to process data continuously, while running eight times slower than real time.

A third generation of changes were introduced in 1985 (Figure 3). The PDP 11/40 computer was changed to a PDP 11/34* with a floating point processor, and more memory. (Neither of these two features is significant for this application, but they made the computer more generally useful.) An 80 mega-byte disk drive was added along with a high-density cartridge tape unit for archiving and back-up. Simplifications to the algorithm introduced in

---

* Trade mark of Digital Equipment Corporation.
† Trade mark of CSP Inc.
** Unpublished communication.
* Trade mark of Digital Equipment Corporation.

the last generation permitted a re-structuring of the algorithm and streamlining of the software (27). As a result of these changes, the program now runs in real-time for some combinations of parameters. Inexplicably, the system still crashes occasionally, and the cartridge tape back-up unit has proved to be unreliable.

This report discusses results achieved with the most recent versions of the hardware and software.

2. Characteristics of Doppler Ultrasonic Signals

To design an algorithm to detect and count bubbles, it is necessary to compare the characteristics of the Doppler ultrasonic signals scattered by bubbles with those of the normal scatterers such as red blood cells.

Belcher (22) adopted a simple model of the bubble signal consisting of a pure sine wave modulated by a Gaussian envelope – a tone burst. This model would apply when a bubble passes with constant velocity through an ultrasonic beam having a Gaussian spatial variation in intensity. Kisman (23) modelled the bubble signal as a transient event with a duration from 10 to 20 ms.

How well do these models reflect what is observed? The actual signals are complicated, and depend on the conditions of measurement. For human subjects, several measurement sites (12) may be used. The most important of these is the precordial site (the right heart and pulmonary artery), but observations are also commonly made at veins such as the subclavian veins and the inferior vena cava. For animals, transducer probes are sometimes implanted around major veins and arteries.

Another source of variation in the signal is movement of the subject. In some protocols, the precordial signal is recorded with the subject standing at rest, and again, after the subject has done a deep knee-bend (squatting down and standing up in a slow continuous motion). This movement causes a brief increase in blood flow and may provoke a shower of bubbles if they are present.

2.1. Temporal Characteristics

Listening to Doppler ultrasonic signals from numerous subjects reveals a wide range of characteristics, as illustrated in Figures 4-6. These figures are photographs of oscilloscope traces of tape-recorded Doppler ultrasonic signals for two subjects. They were obtained as follows: The operator viewed the signal on an oscilloscope while also listening to it over speakers. When he heard signals of interest, he triggered the digital oscilloscope to capture and store a record of data. Fig. 4(a) shows the precordial signal for a pre-dive reference recording for Subject 1. The duration of the record shown is 500 ms, long enough to capture most of a cardiac cycle. The higher-amplitude portion at the beginning of the photograph corresponds with systole. It has a characteristic thumping sound. In Figure 4(b), a prominent bubble appears near the middle of the heart beat. Because of its occurrence during the quieter part of the heart beat, it is easily discernible. The duration of this bubble event is at least 50 ms, much longer than the 10 ms reported by Kisman. Bubbles such as this sound like a whistle. In Figure 4(c), a single bubble is seen for the precordial location after movement. Here the duration of the event is about 20 ms. Sounds associated with these bubbles can be described as chirps. When numerous bubbles are present, as in Figure 4(d), the signal is much more complicated. This example represents Grade III (10) (12) (see

Appendix A) precordial bubbles after movement. Here the bubble signals have begun to override the normal cardiac signal. The result is a staccato sound, sometimes with a wet or sloshing background sound. Fig. 5(a) shows signals obtained while monitoring the subclavian vein when bubbles were present. Here the bubble sounds can be clearly distinguished above the soft, windy sound caused by the flow of venous blood. For the subclavian veins, the duration of the bubble transients is longer, typically about 75 ms. The bubbles are clearly audible and produce a clicking or popping sound. Fig. 5(b) shows a subclavian signal when bubbles are numerous. On this oscilloscope trace, it is no longer possible to distinguish individual bubbles. The signal sounds like a loud, rolling, drum beat.

Fig. 6(a) shows the precordial reference signal for a different subject, Subject 2, whose normal precordial sounds are very different from those of Subject 1. For this subject, the overriding feature is the thumping heart wall sound at the beginning of each heart beat. There is no liquid flowing sound. When precordial bubbles are present, as in Fig. 6(b), the character of the signal changes radically. It now sounds much less harsh; it sounds wet, with individual bubble sounds superposed. Finally, Fig. 6(c) again illustrates the case of numerous (Grade III) bubbles, in which the bubble sounds dominate.

These examples show that the picture of bubble signals in the time domain is complex. When bubbles are few it is appropriate to consider them as transients, but when they are numerous this model is no longer applicable. Furthermore, when the bubble events can be distinguished, their duration appears to be from 25-75 ms, longer than the 10-20 ms reported by Kisman (23). Belcher's model of a bubble signal as a sine wave modulated by a Gaussian envelope is too simple, because the intensity of the ultrasonic field is not uniform, or smoothly varying, and the speed of the bubble changes with time as does that of the blood. Nevertheless, this model is a good beginning, and may be appropriate for the case of single, well-defined bubbles, that produce whistle-like signals.

2.2. Averaged Spectral Characteristics

The characteristics of typical Doppler ultrasonic signals in the frequency domain are also important, to show whether bubble signals could be separated by filtering. For the following examples, the recorded Doppler signals were played back to a signal analyser*. The instrument was set up to display average values of the autospectrum, (also known as the power spectrum or periodogram) assuming a random signal. The sampling rate was 25.6 kHz. Each record of 1024 samples was 40 ms long, so the frequency resolution was 25 Hz.

Fig. 7(a) shows the average of 100 autospectra for a reference recording of the precordial signal, with Subject 1 standing at rest. The subject is the same as the one whose oscilloscope traces are shown in Fig. 4-5. There is a peak in the spectrum around 0.5 kHz. At lower frequencies the signal decreases rapidly, because the Doppler bubble detector includes a 200 Hz high-pass filter. Above 0.5 kHz the auto spectrum decreases slowly, and flattens out to form a local maximum at 2 kHz. Above 2 kHz it decreases more rapidly. Figure 7(b) shows the average of 50 autospectra of the reference recording for the precordial site, after movement. The main difference is that the peak at 0.5 kHz has higher amplitude. Otherwise this average spectrum is similar to that in the rest case.

---

* Hewlett-Packard Model 5420A.

Fig. 7(c) shows the average of 125 autospectra for the precordial rest case after a dive to 30 msw for 55 min. Numerous bubbles were detected for this case (K-M code 232 Grade III-). The part of the spectrum below 2 kHz virtually overlaps the spectrum for the reference case. Above 2 kHz, however, it falls off more rapidly, giving the local maximum at 2 kHz more prominence. Figure 7(d) shows the average of 50 autospectra for the precordial movement case. Numerous bubbles were heard after the movement (K-M Code 343, Grade III+). The region 1-2 kHz is emphasized compared to the reference case, and above 2 kHz the spectrum drops off more rapidly.

Figure 8(a) shows the average of 10 autospectra for the right subclavian vein with the subject at rest, when no bubbles were detected. The spectrum peaks at 1 kHz. Above this frequency the magnitude falls at a rate of about 10 dB per octave. The autospectrum after movement is similar.

Fig 8(b) shows the autospectrum for the right subclavian vein with the subject at rest, when numerous bubbles were present (K-M Code 342, Grade III+). The peak in the spectrum is more pronounced, and has moved slightly lower, to below 1 kHz. Fig. 8(c) shows the case for the right subclavian after movement provoked a brief shower of many bubbles. The spectrum for this case is broader, with many spikes.

The average autospectrum for Subject 2 is shown in Fig. 9(a) for the precordial rest case. Compared to the first subject, there is a more pronounced maximum at 0.5 kHz, with a rapid drop-off above 1 kHz, and no local maximum at 2 kHz. The autospectrum for the precordial movement case for this subject was similar to that for the rest case.

Fig 9(b) shows the average of 80 autospectra for the precordial rest case when many bubbles were detected (K-M code 243, Grade III). It differs markedly from the reference autospectrum. The main peak is wider, with the maximum still at 0.5 kHz, but significant energy up to 1.5 kHz. Figure 9(c) shows that when movement caused a shower of many bubbles (K-M code 443, Grade IV) the main peak was even broader.

These examples again illustrate the difficulty of the bubble detection task. The spectrum of the bubble signals overlaps that of the normal cardiac sounds, so simple filtering cannot discriminate the bubble signals. The bubble signals may sometimes change the shape of the spectrum, *e.g.*, for Subject 2, but not consistently from one subject to the next.

2.3. Short-Time Spectra

The preceding analysis was based on averaged autospectra. These averages would obscure spectral changes lasting for short times – spectral transients. According to Kisman (23), it would be advantageous to detect bubbles using their transient spectral properties. To verify Kisman's original description of these properties, a further spectral analysis was carried out to search for changes occurring over short time intervals.

The bubble detection program was modified to print out the logarithm of the autospectrum for different window lengths – 512, 256, and 128 samples. (These lengths are the number of samples used in calculating the fast Fourier transform (FFT).) The tape-recorded signals were sampled at a rate equivalent to 12000 samples per second. Autospectra were therefore obtained for durations of 42.8, 21.4, and 10.7 ms. For convenience, the resolution of each of these autospectra was reduced to 16 lines, ranging from 0 to 2812.5 Hz, by combining adjacent lines so that the centre frequency of the remaining lines was not changed. Thus line number one (0 Hz) was summed with one half of line number two, line number

three was summed with one half of line number two and one half of line number four, and so on. (The algorithm for bubble detection, developed by Kisman and Sweeney, disregarded the top half of the useful spectrum (3000 - 5812.5 Hz).) Plots were made, such as the one in Fig. 10, showing the logarithm of the magnitude in each of the 16 spectral lines as a function of time, for 5-second periods. These plots may be called *spectrograms*. The same examples were used as for the previous analyses. A 5-second period was chosen because it was long enough to observe the structure associated with several heart beats, but short enought to examine this structure in detail. As a by-product of this analysis, useful values of the parameters to be used in the bubble detection algorithm were identified.

Fig. 10 shows the reference spectrogram for Subject 1, for the precordial rest case. The energy in the highest frequency, 2812.5 Hz, is plotted at the top, and the energy in the lowest frequency, 0 Hz, is plotted at the bottom. The ordinate for each of these spectral lines covers a range in power spectral density of 40 dB. Parts (a), (b), and (c) illustrate the results for the three different window lengths, corresponding to window durations of about 40, 20, and 10 ms, as described before. From the plots, it can be seen that an almost regular structure, related to the heart beat, is present in all frequencies up to 2800 Hz. The contraction of the heart produces a pronounced maximum in most spectral lines. This is followed by a quieter period. A second hump in the spectrum, progressing in time from the higher frequencies to the lower frequencies, probably results from blood flow building rapidly to a maximum velocity, then slowing as the heart relaxes. The lines from 900 to 1300 Hz appear to have a less well-defined structure, and the lower frequencies have a prominent second hump. This may be caused by the relaxation of the heart. The occasional narrow peaks (in frequency, a few hundred Hz wide) in the region 1000 Hz and up may be contributed by valves. The increased detail from shorter window lengths does not appear to yield much additional information. The 10-ms example seems noisy, and therefore harder to interpret. The presence of well-defined structure in the highest frequency represented suggests that it might be useful to look at higher frequencies as well.

Fig. 10(d) and 10(e) show the 40-ms and 20-ms spectrograms for the precordial movement case, before the dive. There is little change in the structure of the signal from the rest case. Because the heart-rate is higher, the features are compressed slightly. The signals seem to be of higher amplitude and there is a greater proportion of the energy in higher frequencies. It is instructive to note that a tape drop-out shows up dramatically on the 20-ms time scale (Fig. 10(e)) as a sharp reduction in magnitude for all frequencies, but is effectively smoothed out on the 40-ms time scale (Fig 10(d)).

Fig. 11 shows spectrograms for Subject 1 after a dive. There are several bubbles present per heart beat (K-M Code 232, Grade III-). This is again the precordial rest case, and all three window lengths are represented (Fig. 11(a-c)). There appear to be several bubble transients (circled) at middle frequencies. In general, the signal has more transitions which are more leptokuruc, and a less well-defined structure than the reference signal, but the presumed bubble peaks do not exceed the systolic peak. They do not seem to extend above 2200 Hz, and they are up to 100 ms wide. A comparison of the spectrograms for the three window lengths suggests that the lowest resolution may be sufficient. Fig 11(d) shows the medium-resolution spectrogram for the movement case. Here the bubbles are more numerous, and the bubble signals begin to obscure the usual structure of the heart beat. Again the peaks occur between 900 and 2500 Hz.

Fig. 12 shows an example from the subclavian vein for Subject 1. Fig. 12(a) is the medium-resolution spectrogram for a recording when no bubbles were present. The subclavian signal has the appearance of almost white noise, save for some faint peaks caused by scattering from the subclavian artery. When bubbles are present in the subclavian vein, as in Fig. 12(b), they show up as distinct peaks in each of the lines from 200 to 2000 Hz, and especially from 500 to 1500 Hz. As can be seen by looking at the low-resolution spectrogram in Fig. 12(c), the shorter window length may improve the resolution of these peaks slightly. The high-resolution spectrum, however, produces no additional improvement. Fig. 12(d) shows the subclavian signal after the subject caused a shower of bubbles by clenching his fist. This causes an elevation in all lines of the spectrum for a short period.

Fig. 13 presents some examples for Subject 2, who had a markedly different signal. This is again evident in Fig. 13(a) for the precordial rest case. The ventricular contraction produces a sharp, pronounced peak in all lines from 200 to 1800 Hz. A second peak, caused by the relaxation of the heart, can be seen below 750 Hz. Fig. 13(b) shows the precordial movement case before the dive. The flex does not change the signal much, but the main peak is smaller. The signal peaks are leptokurtic below 1000 Hz. The post-dive example in Fig. 13(c) shows the precordial rest case for numerous bubbles (K-M Code 243, Grade III). The peaks are now much broader and go higher in frequency. Presumably, the bubbles passing through after each contraction maintain the signal level. The bubbles are noticeable between 750 and 2600 Hz. For the precordial movement case in Fig. 13(d), the bubbles are so numerous (K-M Code 443, Grade IV), that they obscure the normal cardiac signal over the entire bandwidth. (The low-amplitude part at the beginning of the example was caused by a momentary reduction in signal strength as the heart moved temporarily out of the focus of the ultrasonic probe during the flex. Such changes in signal-level are often encountered in practice.)

As a check that an upper frequency of 2800 Hz was adequate, these examples were reanalysed using a sampling rate of 16 kHz, thus extending the upper frequency to 3750 Hz. Only the most prominent of features in the spectrum could be discerned above 3000 Hz. Bubble information could not be seen in this region, except in the subclavian movement case, where the shower of bubbles produced broad band noise, and this information was not new. Therefore, it seems justifiable to limit the analysis of the spectrum to frequencies less than 3 kHz.

3. Description of the Algorithm

A description of the algorithm as it was originally designed is given by Kisman (13). A detailed description of the current algorithm can be found in the report by Tam, Feather, and Romkey (27). The process is illustrated in Fig. 14. The recorded Doppler signal is played back using a machine with variable speed control, so that the signals can be processed at speeds from real-time to 32 times slower than real time, by halving. The signal is then passed through an anti-aliasing, low-pass filter, with high-frequency cut-off set to one half the actual sampling rate, or less. The signal proceeds to a 12-bit ADC in the array processor. The sampling rate is selected under program control, taking into account the playback speed of the tape recorder. The data samples are windowed (assembled into one-dimensional arrays). The length of the window is specified at run-time, and can be set at values from 64 to 1024 by doubling or halving. The autospectrum is calculated for each window. The resulting spectrum would be the same length as the original time series, but

the high-frequency half of the spectrum is redundant because it is a reflection of the low-frequency half. The remaining spectrum ranges from 0 Hz to one-half the sampling rate – typically set at 12 kHz. In the original algorithm Kisman (13) used only the lower half of the remaining spectrum. As was shown in the last section, there is little information in the spectrum above 3 kHz. Therefore this was a good choice to save computation time, and has been retained in the current version. The result is a spectrum one quarter of the length of the original time series.

This power spectrum is then multiplied by a filter, to amplify those frequencies where the bubble transients are most likely to be found. The coefficients of the filter are read from a file at run time.

The filtered power spectrum is then used to calculate a transient spectrum, described in greater detail below. The transient spectrum is derived by forming the differences between the current and the preceding, and the current and following spectra, and combining the results, modified by a variable scale factor that is intended to compensate for shifts in the level of the entire spectrum.

The resulting transient spectrum is then compared with a threshold, T, also set at run time. If the threshold is exceeded, a bubble is deemed to have occurred, and a counter is incremented. Cumulative bubble counts are displayed periodically and sent to a file for later analysis. If desired, bubble counts can be displayed for each spectral line .

Figure 15 (27) shows the steps of the algorithm in greater detail. The ADC produces data in integer format, so the next step is to convert the data to floating-point format. After a buffer of samples has been collected, the Fourier transform of the series is computed using the FFT algorithm supplied with the software for the array processor. By multiplying the resulting series of complex numbers by its complex conjugate, the autospectrum (power spectrum), a one-dimensional array of real numbers, is obtained. This is then multipled by the array of filter coefficients.

The filtered autospectrum is then scaled as follows.

$$S_j=G_j/[G+\alpha(G_j-G)+\beta] \tag{1}$$

where G_j is the j'th component of the power spectrum, G;

$$G=(4/N)\sum_{j=1}^{j=N/4} G_j; \tag{2}$$

N is the original series length; α is the specific components weighting factor; and β is the baseline for transient spectrum scaling.

The baseline, β, is usually set to a small number, *e.g.* 1 to ensure that the denominator is never zero. If α is set to 0, then $S_j=G_j/G$, *i.e.*, the scaled spectrum is just normalized by the total power in the signal. This would tend to wipe out differences caused by an global increase in power, and hence would disregard the remarkable scattering efficiency of bubbles (28). If α were set to 1, then $S_j=G_j/(G_j+\beta)$, and if β is negligible, there is no scaling at all. Usually, α is set to about 0.4.

Next forward and backward *transient* spectra are calculated as follows. The forward transient spectrum is given by

$$H_{j_k}=S_{j_k}-S_{j_{(k+1)}}, \tag{3}$$

and the backward transient spectrum is given by

$$B_{j_k}=S_{j_k}-S_{j_{(k-1)}} \tag{4}$$

Each of these transient spectra is compared with a threshold. A bubble is counted for each spectral line of both the forward and backward transient spectra that exceeds the threshold.

To minimize the number of operations required, the algorithm is computed in a slightly different way, but the effect is the same. Figure 15 shows that the scaling is applied after the difference has been computed. The difference need be computed only once. It is saved, and the next time through the loop, becomes the backward difference. There must always be a delay of two loops before counts are produced. The forward and backward difference spectra are compared with the threshold to produce two logical arrays of *TRUE* and *FALSE* values. The results are then combined using a logical *AND* on each component. Each remaining *TRUE* value is counted as a bubble.

Earlier versions of the algorithm (13) were more complicated. In these versions, two overlapping series of transient spectra were calculated to guard against the occurrence of bubbles midway between two blocks of data. A third, longer transient spectrum was computed to detect longer duration bubbles. The results of the three parallel comparisons were compared to a look-up table to estimate the number of bubbles present. Experience has shown, however, that this complexity is unnecessary. It turned out to be impracticable to detect every bubble since, as was shown in the preceding section, the bubbles can be so numerous that their signals are not physically distinguishable. The current algorithm cannot yield an accurate bubble count, but produces a count related to the number of bubbles present. The tests described in the next section were carried out to describe the sensitivity, reliability, and validity of the algorithm for detecting bubbles.

4. Tests of the Algorithm

4.1. Methods

The algorithm, in its various versions, has been tested many times. It was necessary to determine good values of the parameters of the algorithm for bubble detection, and to describe its performance. These tests have been carried out with simulated signals and with real data from both animals and man (13).

Precordial signals from man provide the most difficult test. As there is no independent way of establishing the number of bubbles present in the test signals, it was necessary to compare the performance of algorithm with bubble grades assigned by independent observers (12). These bubble grades constitute a signal classification, rather than counts, but they give rough indications of the number of bubbles present. The comparison was therefore qualitative at best.

Tests of the algorithm were complicated by the number of parameters to vary. Even in the latest, simplified version, there are six, listed in Table 1.

Table 1. Parameters of the Algorithm

Description	Symbol	Initial Value
detection threshold	T	25.0
filter file		flat 500-3000 Hz
transient spectrum weighting factor	α	0.4
transient spectrum baseline	β	1
sampling frequency		12.8 kHz
buffer size		256

Some of them, such as buffer size and sampling frequency, are interrelated, and have only a few permissible values. On the other hand, the filter shape is a one-dimensional array of coefficients, length depending on buffer size, offering a huge range of possible choices.

In the results to follow, we have concentrated on tests using the same two subjects as in the earlier section on the characteristics of Doppler ultrasonic signals. These subjects provided signals representing a range of individual characteristics and a range of bubble counts. They provided a difficult but realistic test.

The recorded signals were played back, usually slowed down by a factor of two. When the sampling frequency was specified as 12.8 kHz, therefore, the actual conversion rate of the ADC was 6.4 kHz. The analysis was carried out for the same length of time as used by the human observers to produce bubble grades. These bubble grades were assigned previously using the *K-M Code* (9) (10) (12). (Appendix A describes this code.) The output from the bubble detection algorithm was stored in a file as total counts per second and counts per second for each spectral line. The results were then transferred to a VAX* super-minicomputer running UNIX† and analysed using the statistical packages *S*† (29) and *BMDP* (30).

4.2. Results

4.2.1. Results for the initial parameter set

A series of tests was done with the parameter values shown in Table 1. The first of these tests used the pre-dive reference recording of the precordial signal for Subject 1, while he stood at rest. There were seventeen counts, presumed to be false, during the 15-second recording, a mean of 1.13 counts per second, or roughly one count per heart beat (standard error (s.e.) 0.32). Figure 16 shows the histogram of the counts. Each bar shows the absolute frequency of occurrence for each of the counts along the bottom. Counts were reported for one-second intervals. The histogram shows that the most frequently occurring count was zero, but there were a few instances of one's and two's, and one instance each of three and four events per second. Figure 17, a *spectrogram* of the counts, shows that most of the them occurred for frequencies below 1 kHz.

For the pre-dive reference recording of the *precordial movement* case, there were 27 counts in 31 seconds. The mean frequency of counts is slightly less for this case (mean

* Trademark of Digital Equipment Corporation

† Trademark of Bell Laboratories.

0.87, s.e. 0.22). It is the total count that is most important for the movement case, however, since this case produces, by design, a nonstationary signal (12). The histogram (Figure 18) of bubble counts shows that there are a few more instances of higher counts. Most of the counts occurred below 800 Hz.

In the post-dive evaluation of the *precordial rest* case for this subject, the observers assigned K-M Code 232. This means that there were usually a few bubbles per heart beat, and they were not as loud as the background cardiac signal. The mean frequency of bubble counts detected by the algorithm was 1.29 counts per second (s.e. 0.18). This is not much greater than the pre-dive mean. A comparison of the pre- and post-dive cases using the Kruskal-Wallis one-way analysis of variance based on ranks, shows that the means were not significantly different (p=0.63). The use of statistics based on ranks is appropriate because the data are not normally distributed, and no normalizing transformation could be found. Therefore they do not meet the criteria required for the standard analysis of variance (31). Nevertheless, the histogram (Figure 19) shows that *one* is now the most frequent count, and the spectrogram (Figure 20) shows that there were many more counts at higher frequencies.

For the *precordial movement* case, the diver did two repetitions of a knee-bend, 30 seconds apart, followed by two flexes of both arms. The observers graded each repetition. The last of these was classified K-M Code 343. This means that the observers heard more than 9 (but probably less than 40) bubbles per heart beat, in more than 10 consecutive heart-beats, and they were about as loud as the cardiac sounds. The algorithm counted 60 bubbles in 26 seconds during the same flex. This is fewer than the observers felt were present, but more than the number of counts detected in the reference case (27 in 31 seconds). Figure 21 shows the histogram of these counts. The Kruskal-Wallis test showed that the pre- and post-dive means were different (p=0.0032).

For this diver, one subclavian vein was given Grade **0** by the observers, for both *rest* and *movement*. The algorithm produced one count for the rest case. This was caused by a transient noise spike, easily identified as such by the human observers, but not by the algorithm.

For the other subclavian vein, the observers classified the signal as K-M Code 342, meaning they heard more than 9 bubbles per second, continuously, and the signal was moderately loud. The algorithm produced a mean count of 1.65 bubbles per second (s.e. 0.30). The histogram is shown in Figure 22. Figure 23 shows that these counts were all below 1200 Hz, extending down to 500 Hz.

When the subject was asked to clench his fist, a brief shower of bubbles was produced, graded by the observers as K-M Code 413. The algorithm was insensitive to this shower. It produced bubble counts of 2, 4, and 9 for the three flexes. The reason for this insensitivity can be traced to the underlying model of bubble events as transients. When the bubbles are so numerous that they can no longer be distinguished individually, the isolated-transient model is no longer valid. The algorithm treats the signal as continuous noise – something it was designed to reject.

The second subject's reference *precordial* signal at rest was different in sound from that of the first subject. It was a harsh, dry-sounding signal, and the heart rate was high – about 120 per minute. Figure 24 shows the histogram of bubble counts for the precordial reference signal for that subject. The mean frequency of counts for him was 2.05 (s.e. 0.33), about twice the frequency of the counts for the reference recording of the first subject. This

might be attributable to the higher heart rate. Figure 25, the bubble count spectrogram, shows that all of these counts were in spectral lines below 850 Hz.

The post-dive signal for this subject was graded by the observers as K-M Code 243, meaning that there were 3-9 bubbles counted in every heart beat, and that the signals were as loud as the cardiac sounds. The algorithm produced a mean count of only 1.56 per second (s.e. 0.18). This is lower than the reference case, but the Kruskal-Wallis test shows that the means are not significantly different (p=0.39). The lower counts may be attributable, in part, to a lower heart rate, post-dive. The bubble counts histogram (Figure 26) shows that the most frequent count was two per second, and the bubble counts spectrogram (Figure 27) shows that several counts now appeared in the region between 850 and 1550 Hz. Between the pre-dive and post-dive recordings, the signal changed dramatically. The harsh, staccato pre-dive signal was replaced by a slow, sloshy signal. This wet sound is often associated with bubbles.

4.2.2. Effect of filter

This set of examples suggested that the number of counts for the reference case should be reduced if the spectral lines below 850 Hz were ignored. Therefore, the same set of tests was run with the low-frequency cut-off raised from 500 to 800 Hz. With this choice, the filter was therefore flat from 850 to 3000 Hz.

For the reference recording of the first diver, *precordial rest* case, the mean of the counts per second was reduced from 1.13 to 0.82 (s.e. 0.18). Unfortunately, the number of bubble counts in the post-dive recording was also reduced to 0.77 (s.e. 0.13), so the bubbles were still not distinguished in this case. The Kruskal-Wallis test showed no significant difference in the means for the pre- and post-dive cases (p=0.49). Also the differences between the two pre-dive cases for the different filters were not significant (p=0.66), but the differences between the two post-dive runs were significant, (p=0.0081).

Two unexpected effects were noticed. The most frequent count per second was one in this case, whereas it had been zero with the other filter. This means that the lower mean was achieved by reducing the number of instances of multiple counts per second. This can be seen by comparing Figure 28 with Figure 16. Second, a comparison of Figure 29 with Figure 17 shows that the number of counts in the region above 850 Hz increased, although the filter coefficients and thresholds were not changed in that region. This can be attributed to the indirect influence of α. By reducing the width of the spectrum the total power, G, in Equation 1, is reduced. The scaled spectrum is therefore increased unless α=1.0.

As was expected, this filter produced poorer subclavian results, because most of the subclavian signal is concentrated at lower frequencies. This suggests that a different set of parameters would have to be used for venous signals.

The filtering appeared to be more effective for the second subject. For him, the average frequency of counts for the reference recording was reduced to 0.455 per second (s.e. 0.17) from 2.05 per second, for the *precordial rest* case. According to the Kruskal-Wallis test this difference was significant (p<0.0001). The average counts per second for the post-dive signal stayed almost the same – 1.58 (s.e. 0.21) vs. 1.56 earlier. The difference between the pre- and post-dive cases was now significant (p=0.0002). Improvements were also observed for the *precordial movement* case for this subject, but, perhaps because of the swamping effect of the many bubbles, the improvements were smaller.

4.2.3. Effect of threshold

The above observation that reducing the bandwidth effectively reduced the threshold for bubble counts, for α=0.4 suggested another series of tests with the threshold doubled from 25.0 to 50.0 to compensate. For the *precordial rest* case for Diver no. 1, the average rate of counts for the reference recording was reduced to 0.176 (s.e. 0.128) from 0.824 (s.e. 0.177) per second. The differences are significant (p=0.0031). The post-dive counts were still only 0.143 (s.e. 0.059), so bubbles were not distinguished. The ratio of post-dive to pre-dive counts was improved for the *precordial movement* case for three of four *flexes*, however. The ratios were 1.2, 6.7, 9.3, and 10.4, and the improvement for the last three was about three times. On the other hand, the differences between mean post- and pre-dive bubble counts were smaller for the higher threshold. According to the Kruskal-Wallis test both the differences between the two thresholds and the differences for pre- and post-dive counts were significant (p<=0.0009).

For the second diver, the increase in the threshold for bubble counting had a less clear effect. For the *rest* case the performance was decreased, and bubbles were no longer distinguishable, but for the *movement case*, the relative performance was improved, because the reference counts were reduced to zero. This shows that different sets of parameters would be needed for each subject, and for each condition.

4.2.4. Effect of α

As described in the previous section, the parameter α is meant to compensate for level shifts affecting the entire spectrum. By reducing α from 0.4 to 0.2, such level shifts should have less influence, while an increase to 0.8 should produce greater sensitivity to level shifts. Table 2 shows a comparison of the counts observed for the 19 test cases for three values of α: 0.2, 0.4, and 0.8. The results were ranked according to the difference between the counts observed for the post-dive and the reference cases; the greatest difference was ranked one. The reference cases were ranked according to the number of counts; the case with the fewest counts was ranked one. Table 2 shows that on a case by case basis, it was difficult to discern whether one choice produced better results than another. When all 19 cases were ranked, α=0.2 had the best score, but the differences were not significant according to the Kruskal-Wallis test (p=0.49).

4.2.5. Effect of β

The main function of the parameter β is to ensure that the denominator in Eq. 1 is never zero. If β were chosen small enough, *e.g.*, β=1, it should have little influence. To test this assumption the tests were run for β=1 and β=10. Slightly different counts were obtained for each case, but the differences were not significant (p=0.78).

4.2.6. Effect of sampling rate

To determine the effects of sampling rate on the performance of the algorithm, the sampling rate was varied from its initial value of 12.8 kHz to 15.4 and 7.7 kHz. No systematic differences were found for the three sampling rates, either by considering the counts for the 19 cases, or the differences between pre- and post-dive counts (p=0.97 and p=0.12).

4.2.7. Effect of buffer size

The buffer size defines the duration of the window used for comparing transient spectra. Comparisons were made for three buffer sizes, 128, 256, and 512 samples, corresponding to window durations of 10, 20, and 40 ms. Thus the number of windows per second is inversely related to buffer size. On the other hand, the number of spectral lines is equal to one quarter of the buffer size. Since bubble counts are made for each spectral line, the maximum bubble count remains constant as the buffer size is varied, if the filter coefficients are changed to reflect the altered resolution. (If all coefficients are 1.0, this maximum is 3200.) A comparison of the total counts for each of the three buffer sizes shows significant differences (p=0.01). Higher counts were obtained for the larger buffer sizes. However, a comparison of the differences between post- and pre-dive counts does not produce significant differences (p=0.70).

Table 2. Results of varying the specific component weighting factor, α

Case	K-M Code	α								
		0.2			0.4			0.8		
		count	dif*	rank	count	dif	rank	count	dif	rank
Diver # 1										
pr	ref	1		1	3		2.5	3		2.5
pm	ref	2		1.5	2		1.5	5		3
pr	232	13	12	1.5	8	5	3	15	12	1.5
pm	233	3	1	2	2	0	3	8	3	1
pm	232	5	3	3	9	7	1	10	5	2
pm	343	15	13	1	14	12	2	14	9	3
pm	343	4	2	3	11	9	1	9	4	2
sr	0	0		2	0		2	0		2
sm	0	0		2	0		2	0		2
sr	342	4	4	2	2	2	3	7	7	1
sm	413	2	2	1	0	0	3	1	1	2
sm	413	0	0	2	0	0	2	0	0	2
sm	413	4	4	1	1	1	2.5	1	1	2.5
Diver # 2										
pr	ref	0		1	6		3	5		2
pm	ref	6		2	0		1	12		3
pr	243	8	8	2	7	1	3	17	12	1
pm	443	5	-1	3	3	3	2	16	4	1
pm	443	19	13	2	14	14	1	11	-1	3
pm	443	19	13	2	14	14	1	11	-1	3
rank sum				35			39.5			39.5
final rank				1			2.5			2.5

Explanation of symbols: * dif is the number of counts post-dive - number of counts for the reference case; p – *precordial*; s – *subclavian*; r – rest; m – movement.

5. Discussion

The results reported in the previous section show that the algorithm was capable of "detecting" bubbles at least some of the time, *i.e.* the program yielded a significant increase in the number of bubble counts for the post-dive evaluations when compared with the pre-dive reference evaluation for the same case. If the algorithm were to be used operationally, a pre- and post-dive comparison mechanism would be required.

Unfortunately, the parameters of the algorithm have to be tailored to the specific type of evaluation and to the individual diver. This is undesirable because an acceptable combination of parameters may not be known in advance. The filter shape and thresholds have the greatest influence on the results. The other parameters could be set to reasonable values and treated as constants. It appears valid to ignore frequencies above 3 kHz. For venous signals, a lower range of frequencies is required, *e.g.* 300–1500 Hz, compared with precordial signals, *e.g.* , 850–2500 Hz.

Although the algorithm may be successful when the rate of bubble production is moderately high, and it could be argued that failure to detect bubbles when they are infrequent is unimportant, a more serious problem arises when bubbles are numerous. The algorithm may then fail to detect bubbles at all. The reason for this failure is that the model of bubbles as transients is no longer valid. A better description of the bubble signals would then be continuous noise – something the algorithm was designed to reject. A more acceptable behaviour would be saturation at a maximum count, rather than diminishing to zero for the case of very many bubbles.

Is there a better approach? The complexity and variability of the Doppler signals shows that it would be difficult to devise a simple system that could count bubbles accurately. At one extreme, it is difficult to distinguish the occasional individual bubble from such normal heart sounds as valve sounds. At the other extreme, the bubbles can be so numerous that it becomes impracticable to separate their individual contributions to the acoustic signal, either temporally or spatially. A better approach might be to use pattern matching. This is partly what human observers do. It would be difficult to match the performance of an expert, but it should be possible to program a machine to distinguish three cases: zero or occasional bubbles, frequent bubbles, or many bubbles. The problem is similar to recognizing other complex sounds such as music or speech. One approach that might be fruitful would extract the principal components of the Doppler signal, and attempt to match them to the principal components of prototypes stored in memory.*

What is really required of a practical system? Even one capable of successfully recognizing bubble signals with as much proficiency as a human expert would still require human intervention to acquire the signal in the first place. Once an individual has been taught how to acquire a good signal, it usually is not difficult to teach him to grade the signal. Indeed, to become proficient at acquiring good Doppler signals, one must almost become expert at recognizing the bubbles. Except possibly for long-term, continuous monitoring, *e.g.* , during excursions to a lower pressure from saturation at a higher pressure, there is little reason for a machine to take over the task from a human, unless it can be made more reliable and more sensitive than the human. This is unlikely to succeed without a large research and development effort.

---

* M.M. Taylor, personal communication.

6. Recommendations

The current practice of classifying Doppler ultrasonic signals has some drawbacks. It is subjective and it requires a well-trained and vigilant observer. It is also tedious and labour-intensive. Nevertheless, it is simple and meets DCIEM's need for describing the results of decompression experiments.

Any practical bubble counting system would either require continual human intervention, or a large measure of *artificial intelligence*. In the first case, there is little reason for using the system; it may cost more in time than it is worth. In the second case, the effort required to develop the system would be prohibitive.

At present, it seems best to train the observers well, and monitor the quality of their assessments frequently. A team approach to classification is valuable for ensuring high quality.

The problem of automatic bubble detection in Doppler signals is similar to other signal classification problems that occur, for example, in machine recognition of speech and in detection of targets in audio sonar signals. Therefore, developments made in these areas could be tried on the bubble detection problem.

Acknowledgements

The algorithm was conceived by Kenneth E. Kisman. Bud Rodden helped with the programming for the early versions, especially the nasty assembly language parts. Bill Demmery and Tim Yeung have worked hard to keep the hardware going, especially the troublesome MAP. Jeff Richardson helped with the RT-11 system. Tom Feather and Phil Romkey of Array Systems Computing enhanced the algorithm by streamlining the software. Ron Nishi and our managers have been most patient in waiting for results. We thank all these individuals for their contributions.

REFERENCES

1. Spencer, M. P. Decompression limits for compressed air determined by ultrasonically detected blood bubbles. J. Appl. Physiol. **40**:229-235, 1976.

2. Masurel, G., R. Guillerm, and Cavenal. Détection ultra-sonore par éffet Doppler de bulles circulantes chez l'homme lors de 98 plongées à l'air. Revue de Médecine Subaquatique et Hyperbare, 199-201, 1976.

3. Guillerm, R., G. Masurel, J. Le Pechon, C. Guillaud, and J. Ocana De Santuary. Détection Ultrasonore (Effet Doppler) De Bulles Circulantes Chez L'Homme Pendant La Phase De Décompression D'Une Plongée Simulée A 300 Mètres A Saturation En Atmosphère Oxygène-Helium. Lyon Méditérranée Médical XIII:7-12, janvier 1977.

4. Masurel, G., E. Gras, B. Gardette, A. Ternisien, and R. Guillerm. Détection ultrasonore par éffet Doppler de bulles circulantes au cours de plongées humaines d'intervention Helium-oxygène. Méd. Aéro. Spat. Méd. Sub. Hyp., 131-133, 1977.

5. Kisman, K., G. Masurel, D. LaGrue, and J. Le Pechon. Evaluation de la qualité d'une décompression basée sur la détection ultrasonore de bulles. Méd. Aéro. Spat. Méd. Sub. Hyp. XVII:293-297, 1978.

6. Gardette, B. Correlation between decompression sickness and circulating bubbles in 232 divers. Undersa Biomed. Res. **6**:99-107, March 1979.

7. Nishi, R. Y., K. E. Kisman, B. C. Eatock, I. P. Buckingham, and G. Masurel. Assessment Of Decompression Profiles And Divers By Doppler Ultrasonic Monitoring. in: *Underwater Physiology VII: Proceedings of the Seventh Symposium on Underwater Physiology*, Bachrach, A. J. and M. M. Matzen (eds.), Undersea Medical Society Inc., Bethesda MD, 717-727, 1981.

8. Eckenhoff, R. G. and R. D. Vann. Air and nitrox saturation decompression: a report of 4 schedules and 77 subjects. Undersea Biomed. Res. **12**:41-52, March 1985.

9. Kisman, K. E., G. Masurel, and R. Guillerm. Bubble Evaluation Code For Doppler Ultrasonic Decompression Data. Undersea Biomed. Res. **5**:28, March 1978. (Abstract).

10. Masurel, G. Méthode D'Evaluation Des Degrées De Bulles Circulantes Révellés Par La Détection Ultrasonore A Effet Doppler "Code K.M.". 283 CERTSM , Centre d'Etudes et de Recherches Techniques Sous-Marines, Toulon, 20 juillet 1983.

11. Kisman, K. and G. Masurel. Method For Evaluating Circulating Bubbles Detected By Means Of The Doppler Ultrasonic Method Using The "K.M. Code". . (English translation of 283 CERTSM 1983).

12. Eatock, B. C. and R. Y. Nishi. Procedures for Doppler Ultrasonic Monitoring of Divers for Intravascular Bubbles. DCIEM 86-C-25, Defence and Civil Institute of Environmental Medicine, Downsview, ON, May 1986.

13. Kisman, K. E. Spectral analysis of Doppler ultrasonic decompression data. Ultrasonics, 105-110, May 1977.

14. Smith, K. H. and M. P. Spencer. Doppler Indices of Decompression Sickness: Their Evaluation and Use. Aerospace Med. **41**:1396-1400, December 1970.

15. Nishi, R. Y. and S. D. Livingstone. Intravascular Changes Associated With Hyperbaric Decompression: Theoretical Considerations Using Ultrasound. Aerospace Medicine **44**:179-183, February 1973.

16. Guillerm, R., G. Masurel, M. Monjaret, H. David, and B. Schmidlin. La Détection Ultrasonore Par Effet Doppler Des Bulles Intravasculaires Chez Le Miniporc Après Exposition Hyperbare: Rôle Filtrant Du Poumon. Bulletin Médsubhyp **10**:50, 1973.

17. Guillerm, R. and G. Masurel. Détection Ultrasonore Par Effet Doppler De Bulles Intravasculaires Lors De La Décompression Après Exposition Hyperbare Du Porc Premiers Résultats. 161-CERTSM-73, 16 mai 1973.

18. Monjaret, J., R. Guillerm, and G. Masurel. Détecteur ultrasonore a éffet Doppler de bulles circulantes dans les vaisseaux sanquins. in: *Colloque international sur les capteurs bio-médicaux, Biocapt 75*, Comité d'organisation du colloque international sur les capteurs bio-médicaux, Paris, 93-98, 3-7 Nov. 1975.

19. Moulinier, H. and G. Masurel. Detection of bubbles in blood vessels and the evaluation of their flow. Med. & Biol. Eng. & Comput. **16**:585-588, 1978.

20. Guillerm, R., G. Masurel, C. Guillaud, and J. Monjaret. Détection Ultrasonore Par Effet Doppler Des Bulles Intravasculaires Chez L'Animal Après Exposition Hyperbare. Lyon Méditérranée Médical XI: 30 octobre 1975.

21. Belcher, E. O., J. E. Ehrenberg, and D. W. Lytle. Adaptive Detection of Emboli in Man during Decompression. in: *The 12th UMS Workshop Early Diagnosis Of Decompression Sickness*, Pearson, R. (ed.), 118-139, 12 May 1977.

22. Belcher, E. O. Quantification of Bubbles Formed in Animals and Man During Decompression. IEEE Trans. on Biomed. Eng. **BME-27**:330-338, June 1980.

23. Kisman, K. E. Decompression Bubble Analysis. DCIEM 75-R-1078, Defence and Civil Institute of Environmental Medicine, January 1975.

24. Bendat, J. S. and A. G. Piersol. *Random Data: Analysis and Measurement Procedures*. Wiley, N.Y., 1971.

25. Bendat, J. S. and A. G. Piersol. *Engineering Applications Of Correlation And Spectral Analysis*. Wiley, N.Y., 1980.

26. Sturgess, C. *Gas Bubble Detection Program Final Report*. Human Computing Resources Corp, December 1981. (Report for DSS Contract 4EY.3278023, SN 8EY78-04233).

27. Tam, E. W., T. E. Feather, and P. J. Romkey. *Requirements and Feasibility Study for a Doppler Acoustic Bubble Detector for DCIEM*. Array Systems Computing, Inc, March 1986. (Contract report).

28. Nishi, R. Y. The Scattering and Absorption of Sound Waves by a Gas Bubble in a Viscous Liquid. Acustica **33**:173-179, 1975.

29. Becker, R. A. and J. M. Chambers. *S An Interactive Environment For Data Analysis And Graphics*. Wadsworth, Belmont, CA, 1984.

30. Dixon, W. J., ed., *BMDP Statistical Software*. University of California Press, Berkley, 1983.

31. Siegel, S. *Nonparametric Statistics For The Behavioral Sciences*. McGraw-Hill, N.Y., 1956.

Appendix A. The K-M Code for Describing Doppler Ultrasonic Bubble Data

Parameters

Three parameters are used to describe the bubble signal. Each parameter is assigned a classification from 0 to 4. The first and third parameters, *frequency* and *amplitude*, are identical for the two cases – *rest* and *movement*. The second parameter differs. For the *rest* case, it is called *percentage*, while for the *movement* case, it is called *duration*. The combination of these three parameters yields a three-fold classification, the *K-M Code*, for each assessment. This three-fold classification is reduced to a single *Bubble Grade* by referring to Table A5, p. 24.

Frequency – both cases

The first parameter, *frequency*, represents the number of bubbles per cardiac period. The rules for grading this parameter are listed in Table A1.

Table A1. Frequency parameter

Code	Frequency
0	0
1	1 - 2
2	several 3 - 8
3	rolling drumbeat 9 - 40
4	continuous sound

For code 4, the bubbles are so numerous that they cannot be individually distinguished.

Percentage – rest case

The *percentage* parameter represents the percentage of cardiac periods having a specified bubble frequency. The rules for grading this parameter are listed in Table A2.

For example, if out of 100 heart beats, 1-2 bubbles (*frequency* code 1) were detected in 20 of them, then the *percentage* code would be 2. If 40 heart beats had 1-2 bubbles, and 20 had 3-8 bubbles, then *percentage* code 3 could apply for *frequency* code 1, because over 50 per cent of the heart beats had at least 1-2 bubbles. However, *percentage* code 2 would apply for *frequency* code 2, because between 10 and 50 per cent of the heart beats had 3-8 bubbles. It is often possible to describe the same signal in more than one way.

Table A2. Percentage parameter

Code	Percentage
0	0
1	1 - 10
2	10 - 50
3	50 - 99
4	100

Duration - movement case

The *movement* case is a transient event, while the *rest* case is at least a quasi-steady-state event. Because of this difference, the second parameter for the movement case is *duration* instead of *percentage*. The *duration* is counted as the number of successive cardiac periods following the movement, having at least a specified bubble *frequency* – the first parameter. The first such period must occur within 10 heart beats following the movement. The rules for grading the *duration* parameter are listed in Table A3.

Table A3. Duration parameter

Code	Duration (heart beats)
0	0
1	1 - 2
2	3 - 5
3	6 - 10
4	> 10

For example, if 6-10 bubbles were counted in each of the first four heart beats following the movement, *duration* parameter 2 would apply for *frequency* parameter 3. If the number of bubbles counted per heart beat then fell to 3-5 for the next four heart beats, then *duration* parameter 3 could apply to *frequency* parameter 2, because there would have been at least 3 bubbles per cardiac cycle for 8 heart beats following the *flex*.

Amplitude - both cases

The amplitude of the bubble signal, A_b , is compared to the amplitude of the normal cardiac sounds, A_c, using the rules listed in Table A4.

Usually, these three parameters are evaluated in the order presented here. Initially it may be necessary to replay the recording of the signal several times to classify each parameter, but with practice, the observer should be able to do the classification while recording the signal.

Table A4. Amplitude parameter

Grade	Amplitude
0	no bubbles discernible
1	barely perceptible, $A_b \ll A_c$
2	moderate amplitude, $A_b < A_c$
3	loud, $A_b \equiv A_c$
4	maximal, $A_b > A_c$

The resulting K-M Code is written in the form *fpa* for the rest case and *fda* for the movement case, where the three letters represent the grades assigned for the frequency, percentage or duration, and amplitude parameters, e.g. 112. Table A5 can be used to obtain the global bubble grade corresponding to the K-M Code (e.g. 112 → I).

Table A5. K-M Code → Bubble Grade

fpa	g	fpa	g	fpa	g	fpa	g
111	I–	211	I–	311	I	411	II–
112	I	212	I	312	II–	412	II
113	I	213	I+	313	II	413	II+
114	I+	214	II–	314	II	414	III–
121	I+	221	II–	321	II	421	III–
122	II	222	II	322	II+	422	III
123	II	223	II+	323	III–	423	III
124	II	224	II+	324	III	424	III+
131	II	231	II	331	III–	431	III
132	II	232	III–	332	III	432	III+
133	III–	233	III	333	III	433	IV–
134	III–	234	III	334	III+	434	IV
141	II	241	III–	341	III	441	III+
142	III–	242	III	342	III+	442	IV
143	III	243	III	343	III+	443	IV
144	III	244	III+	344	IV–	444	IV

fp(d)a – K-M Code
f – frequency parameter
p(d) – percentage (or duration) parameter
a – amplitude parameter
g – Bubble Grade

Figure Captions

1. The original version of the signal processor for Doppler ultrasonic bubble detection, 1975-1979. ADC refers to a 10-bit analogue-to-digital converter. DAC refers to a digital-to-analogue converter.
2. The second version of the signal processor for Doppler ultrasonic bubble detection, 1979-1985.
3. The current version of the signal processor for Doppler ultrasonic bubble detection, from 1985.
4. (a) An oscilloscope trace showing a pre-dive reference signal for the precordial site with the subject standing at rest. The duration of the record is 0.5 s.
   (b) An oscilloscope trace showing a prominent bubble signal near the middle of the heart beat. The duration of the bubble's signal is at least 50 ms.
   (c) An oscilloscope trace showing an isolated bubble signal for the precordial site after the subject moved. The duration of the bubble's signal is about 20 ms.
   (d) An oscilloscope trace showing signals from numerous bubbles (Grade III). Here the bubble signal has begun to obscure the normal cardiac signal.
5. (a) An oscilloscope trace of bubbles detected in the subclavian vein. The duration of these signals is longer, about 75 ms.
   (b) Numerous bubbles in the subclavian vein. The signal resembles continuous noise.
6. (a) The reference precordial signal for a second subject. The heart wall signal is more prominent.
   (b) The signal for the second subject when bubbles were present.
   (c) Numerous bubbles overriding the normal cardiac signal.
7. (a) The average of 100 autospectra for the reference precordial signal, for the first subject (Fig. 4(a)) standing at rest.
   (b) The average of 50 autospectra for the reference precordial signal, after movement.
   (c) The average of 125 autospectra for the precordial signal, with the subject standing at rest, when numerous bubbles (Grade III-) were present.
   (d) The average of 50 autospectra for the precordial signal, after movement, when numerous bubbles(Grade III+) were present.
8. (a) The average of 10 autospectra for the subclavian vein at rest with no bubbles.
   (b) The average of 50 autospectra for the subclavian vein at rest when numerous bubbles (Grade III+) were present.
   (c) The average of 10 autospectra for the subclavian vein after movement provoked a brief shower of many bubbles.

9.

(a) The average of 35 autospectra for the precordial signal for the second subject at rest.

(b) The average of 80 autospectra for the precordial signal for the second subject at rest, when many bubbles (Grade III) were detected.

(c) The average of 40 autospectra for the precordial signal for the second subject after movement, when a shower of bubbles (Grade IV) were detected.

10.

(a) A spectrogram showing the logarithm of the magnitude of each of 16 spectral lines from 0 to 2812.5 Hz. The plot should be viewed as 16 separate plots, each on a scale from 75 to 115 dB. This spectrogram illustrates the reference precordial signal for the first subject, standing at rest. It has the lowest resolution in time; the window duration was 40 ms.

(b) The spectrogram for the same signals as shown in part (a), but with the window duration shortened to 20 ms.

(c) The spectrogram for the same signals as in parts (a) and (b), but with the window duration further shortened to 10 ms.

(d) A specrtrogram, with a window duration of 40 ms, for the reference precordial signals for the first subject, after movement.

(e) The spectrogram for the same signals as in part (d), but with a window duration of 20 ms. The deep trough at about 2.2s was likely caused by a tape drop-out.

11.

(a) A spectrogram of the precordial signal from the first subject at rest, after a dive. The window duration was 40 ms. The extra peaks circled may be caused by transient signals from bubbles.

(b) The spectrogram for the same signals as in part (a), but with a window duration of 20 ms.

(c) The spectrogram for the same signals as in part (a), but with a window duration of 10 ms.

(d) A spectrogram of the precordial signal from the first subject after movement, after decompression. The window duration was 20 ms. Many bubbles were present, and the bubble signals have begun to override the normal features of the spectrogram.

12.

(a) A spectrogram of the signal from a subclavian vein of the first subject, when no bubbles were present. The window duration was 20 ms.

(b) A spectrogram of the signal from a subclavian vein of the first subject, when numerous bubbles were present. The window duration was 20 ms.

(c) The spectrogram for the same signals as in part (b), but with a window duration of 40 ms. The bubble signals are not as well resolved in this case.

(d) The spectrogram after the subject clenched his fist, causing a brief shower of bubbles. The window duration was 20 ms.

13.

(a) A spectrogram of the reference precordial signal from the second subject at rest. The window duration was 20 ms.

(b) A spectrogram of the reference precordial signal from the second subject after movement.

(c) A spectrogram of the precordial signal from the second subject at rest after decompression, when many bubbles were present.

(d) A spectrogram of the precordial signal after the second subject moved, provoking a shower of bubbles. The bubble signals obscure the normal cardiac signals.

14. A block diagram showing the steps in the bubble counting algorithm, and where they are carried out.

15. A block diagram showing the steps of the algorithm in greater detail.

16. A histogram of counts for the reference precordial signal for the first subject at rest.

17. A spectrogram showing the distribution of counts vs. frequency for the reference precordial signal of the first subject at rest.

18. A histogram of counts for the reference precordial signal for the first subject after movement.

19. A histogram of counts for the precordial signal of the first subject at rest. The observers classified the signal as Grade III- (KM Code 232).

20. A spectrogram showing the distribution of counts vs. frequency for the precordial signal of the first subject at rest. The signal was classified as Grade III- (KM Code 232).

21. A histogram of counts for the precordial signal of the first subject after movement. The signal was classified as Grade III+ (KM Code 343).

22. A histogram of counts for a subclavian signal of the first subject at rest. The signal was classified as Grade III+ (KM Code 342).

23. A spectrogram showing the distribution of counts vs. frequency for a subcavian signal of the first subject at rest. The signal was classified as Grade III+ (KM Code 342).

24. A histogram of counts for the reference precordial signal for the second subject at rest.

25. A spectrogram showing the distribution of counts vs. frequency for the reference precordial signal of the second subject at rest.

26. A histogram of counts for the precordial signal of the second subject at rest. The signal was classified as Grade III (KM Code 243).

27. A spectrogram showing the distribution of counts vs. frequency for the precordial signal of the second subject at rest. The signal was classified as Grade III (KM Code 243).

28. A histogram of counts for the reference precordial signal for the first subject at rest. The low-frequency cut-off of the filter was increased from 500 to 850 Hz.

29. A spectrogram showing the distribution of counts vs. frequency for the reference precordial signal of the first subject at rest, after the low-frequency cut-off of the filter was increased to 850 Hz.

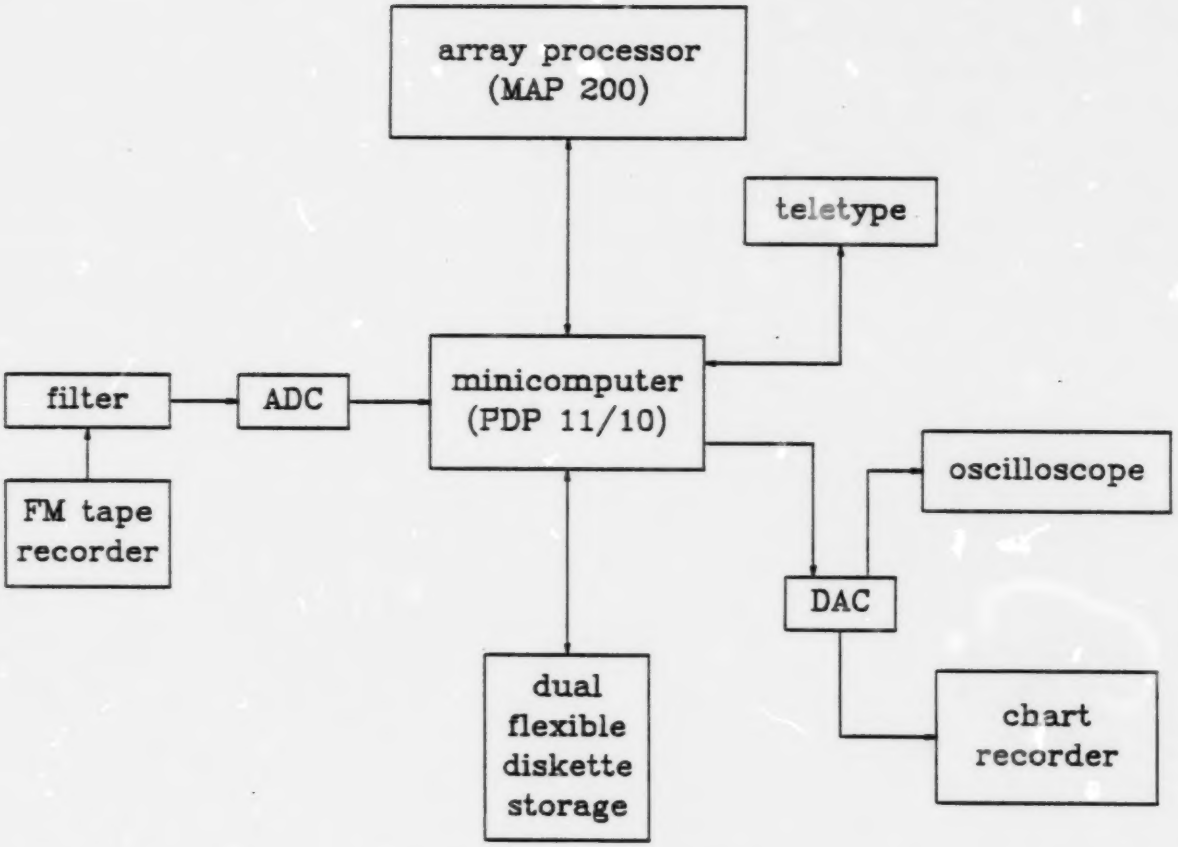

Fig. 1.
The original version of the signal processor for Doppler ultrasonic bubble detection. 1975-1979. ADC refers to a 10-bit analogue-to-digital converter. DAC refers to a digital-to-analogue converter.

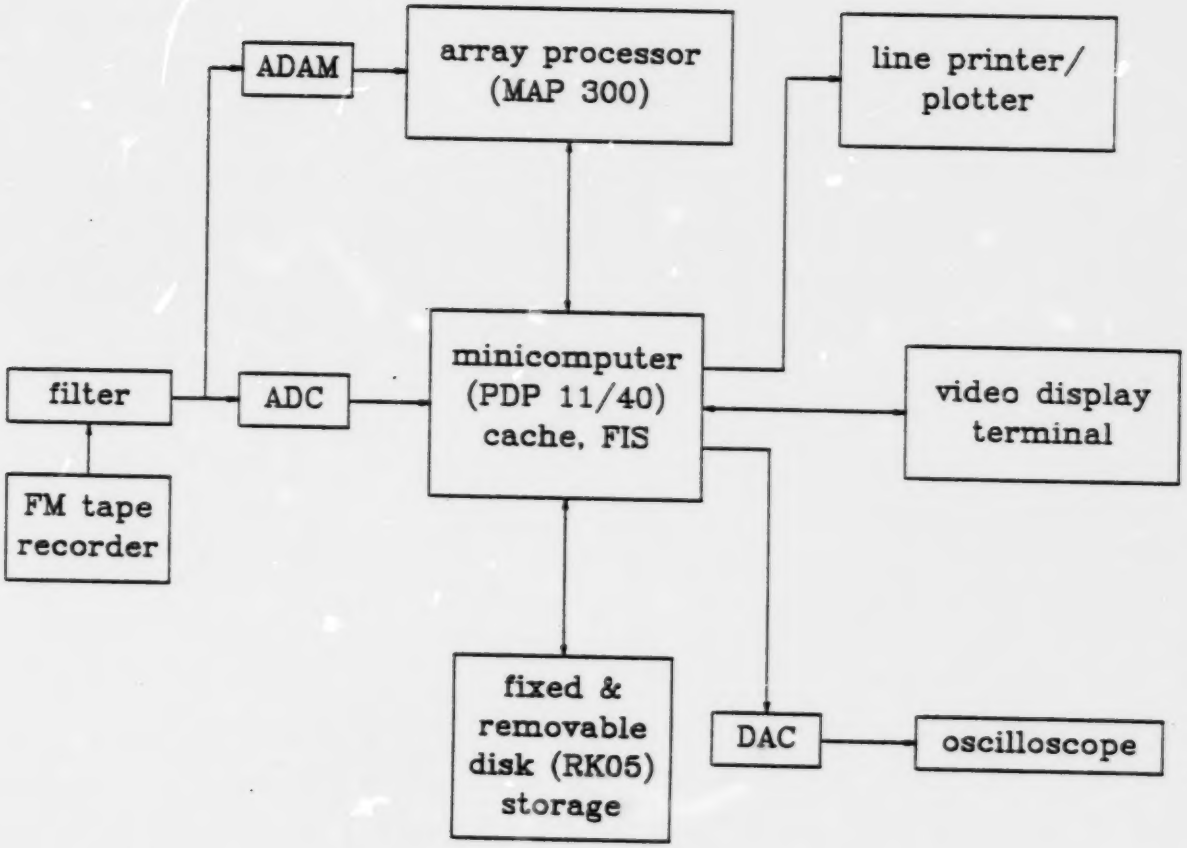

Fig. 2.
The second version of the signal processor for Doppler ultrasonic bubble detection. 1979-1985.

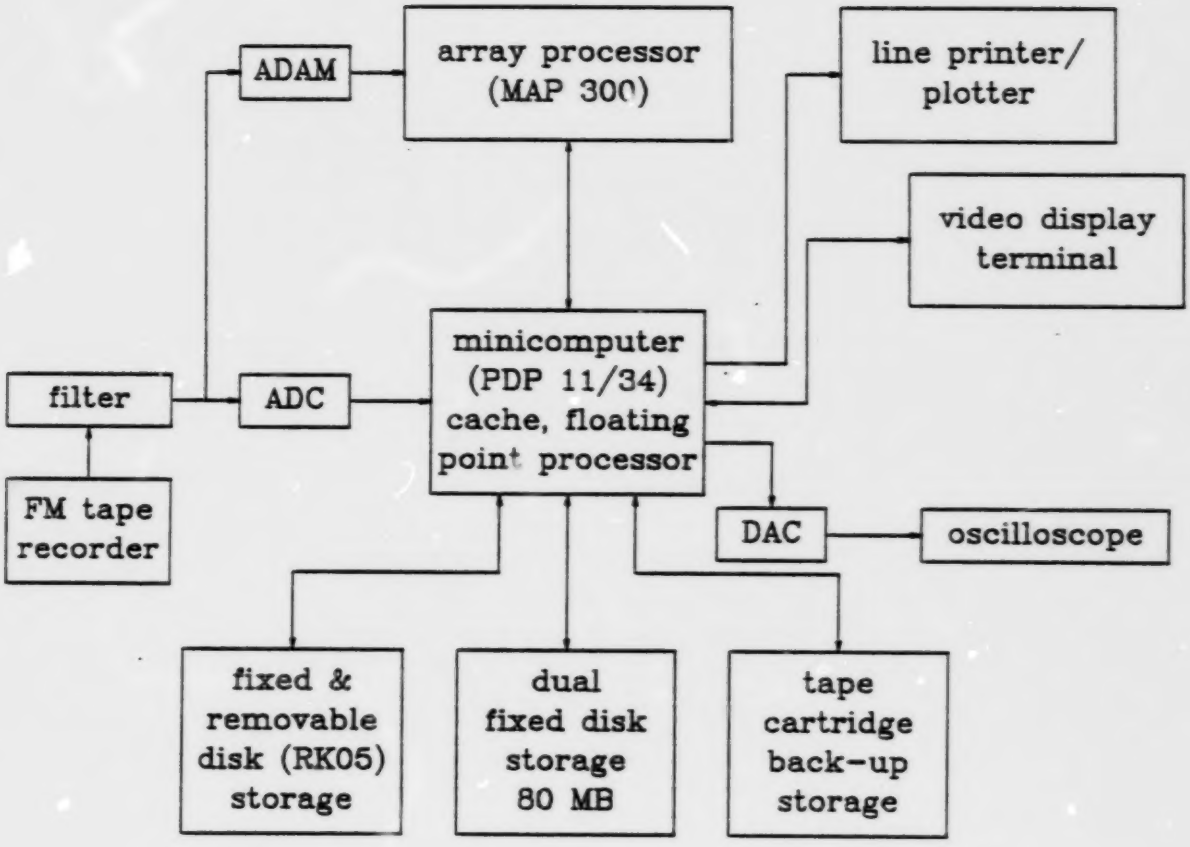

Fig. 3.
The current version of the signal processor for Doppler ultrasonic bubble detection, from 1985.

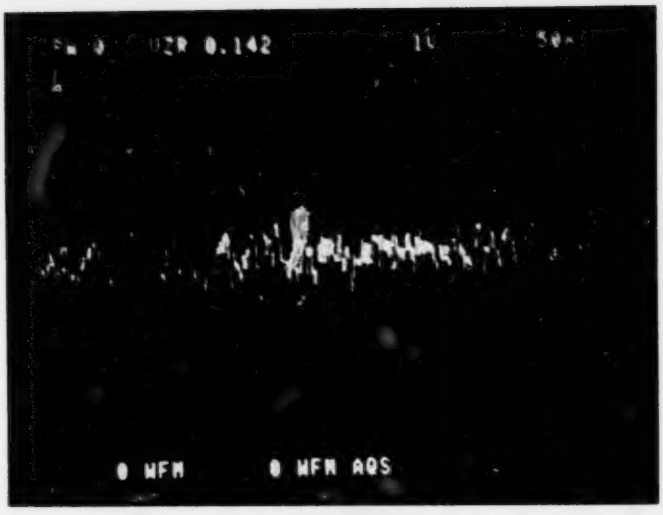

Fig. 4(a)
An oscilloscope trace showing a pre-dive reference signal for the precordial site with the subject standing at rest. The duration of the record is 0.5 s.

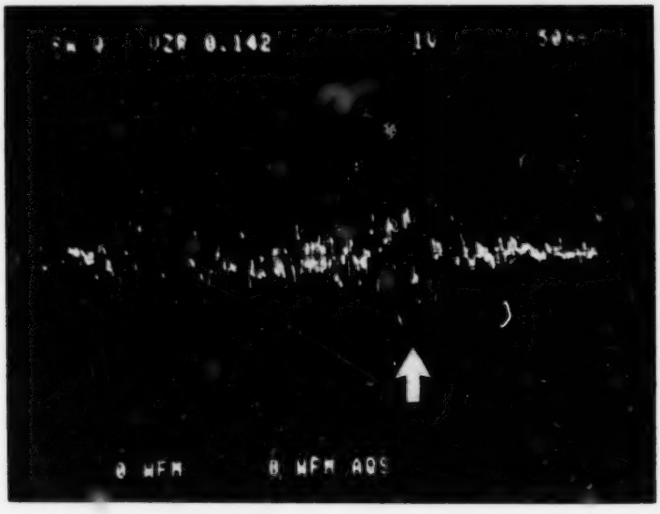

Fig. 4(b)
An oscilloscope trace showing a prominent bubble signal near the middle of the heart beat. The duration of the bubble's signal is at least 50 ms.

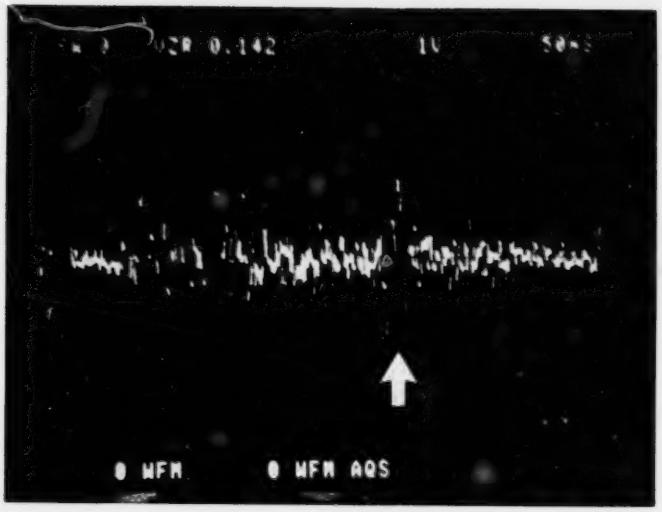

Fig. 4(c)
An oscilloscope trace showing an isolated bubble signal for the precordial site after the subject moved. The duration of the bubble's signal is about 20 ms.

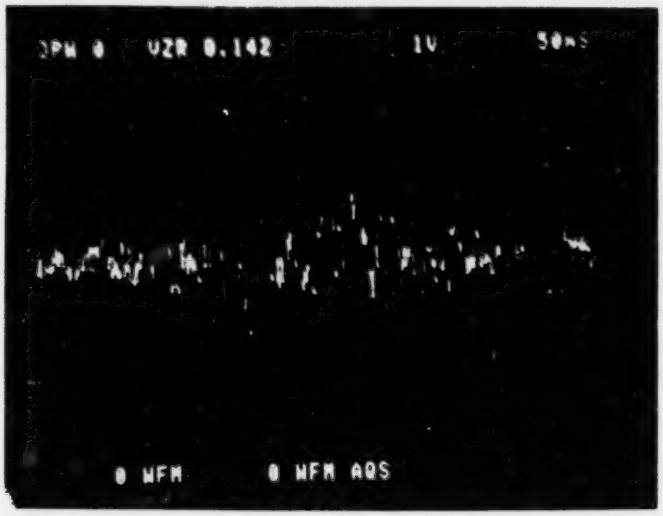

Fig. 4(d)
An oscilloscope trace showing signals from numerous bubbles (Grade III). Here the bubble signal has begun to obscure the normal cardiac signal.

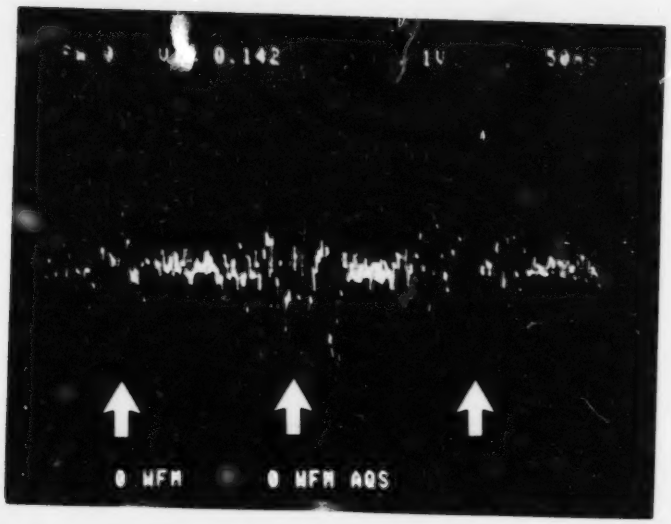

Fig. 5(a)
An oscilloscope trace of bubbles detected in the subclavian vein. The duration of these signals is longer, about 75 ms.

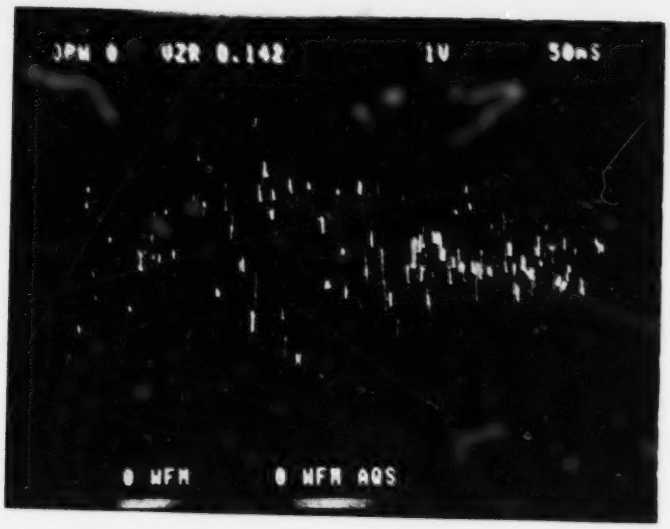

Fig. 5(b)
Numerous bubbles in the subclavian vein. The signal resembles continuous noise.

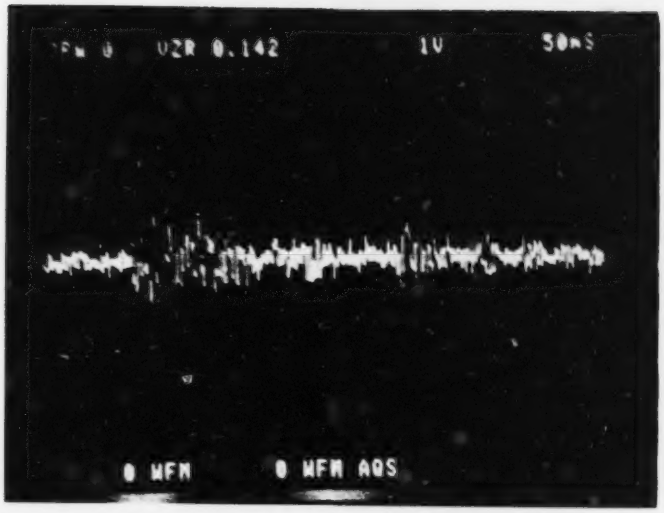

Fig. 6(a)
The reference precordial signal for a second subject. The heart wall signal is more prominent.

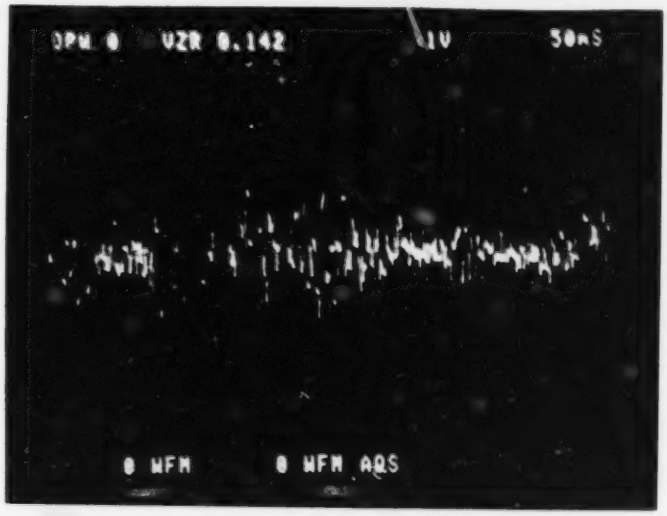

Fig. 6(b)
The signal changed dramatically for this subject when bubbles were present.

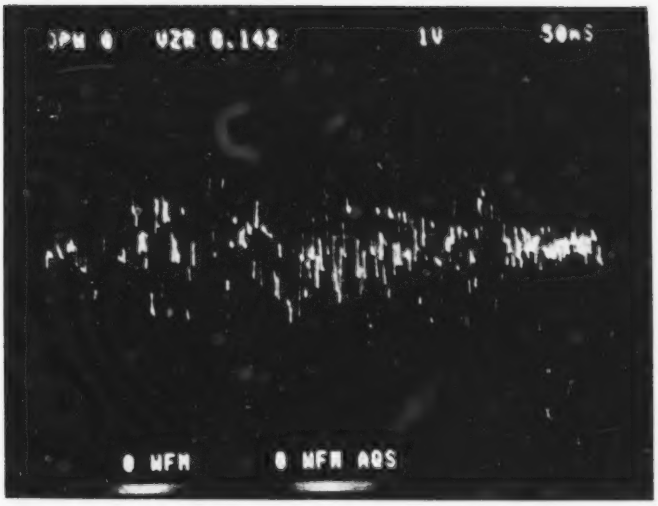

Fig. 6(c)
Numerous bubbles overriding the normal cardiac signal.

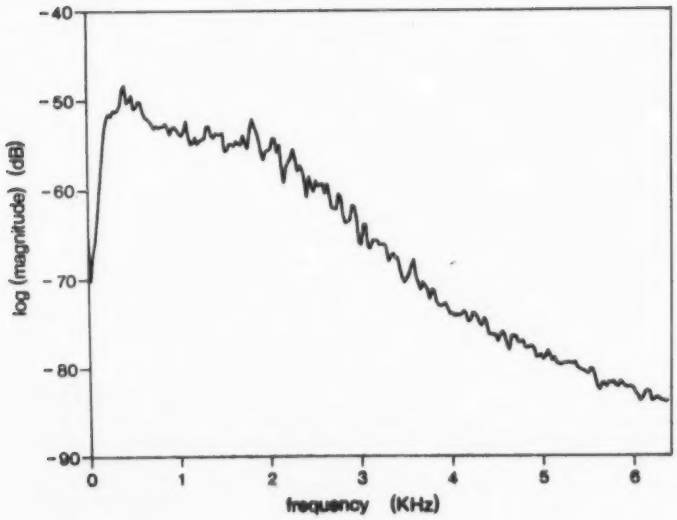

Fig. 7(a)
The average of 100 autospectra for the reference precordial signal, for the first subject (Fig. 4(a)) standing at rest.

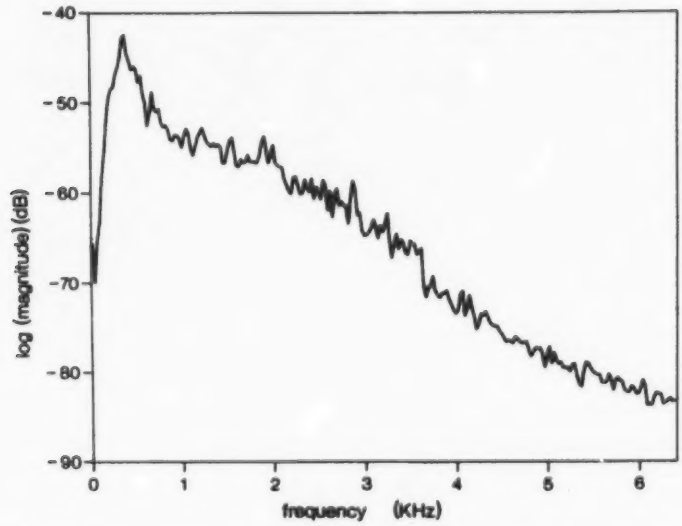

Fig. 7(b)
The average of 50 autospectra for the reference precordial signal, after movement.

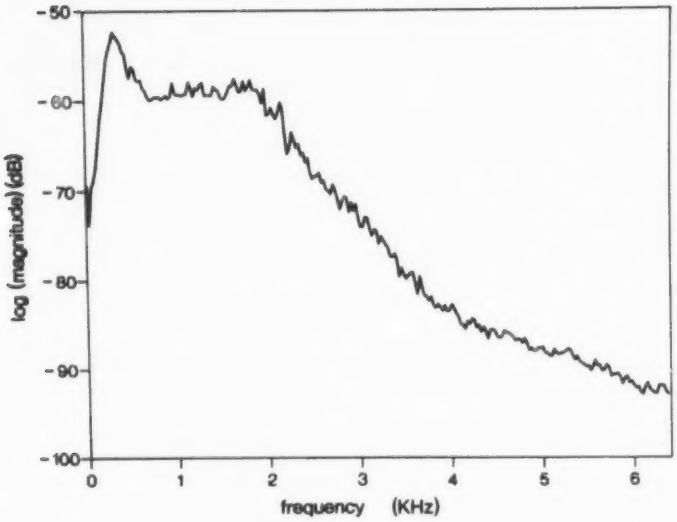

Fig. 7(c)

The average of 125 autospectra for the precordial signal, with the subject standing at rest, when numerous (Grade III-) bubbles were present.

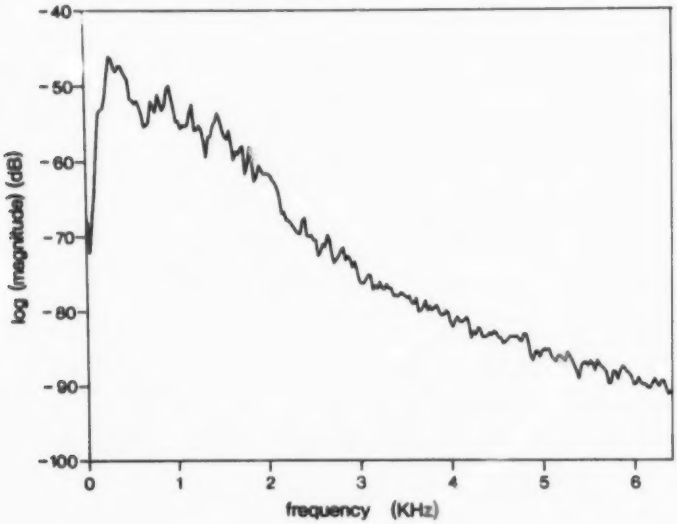

Fig. 7(d)

The average of 50 autospectra for the precordial signal, after movement, when numerous (Grade III+) bubbles were present.

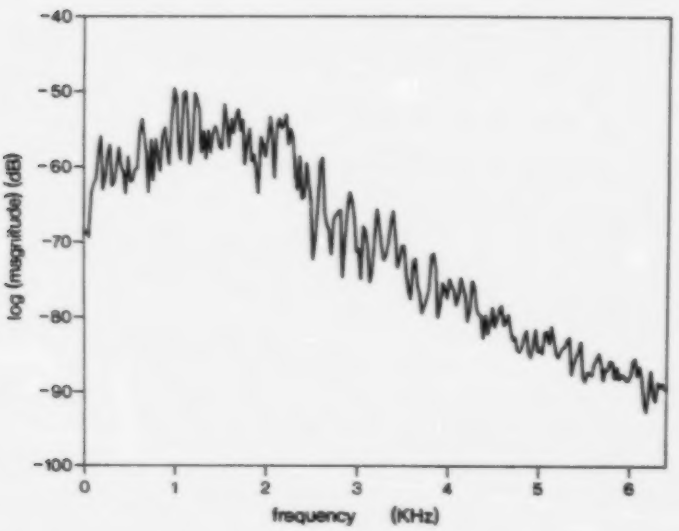

Fig. 8(c)
The average of 10 autospectra for the subclavian vein after movement provoked a brief shower of many bubbles.

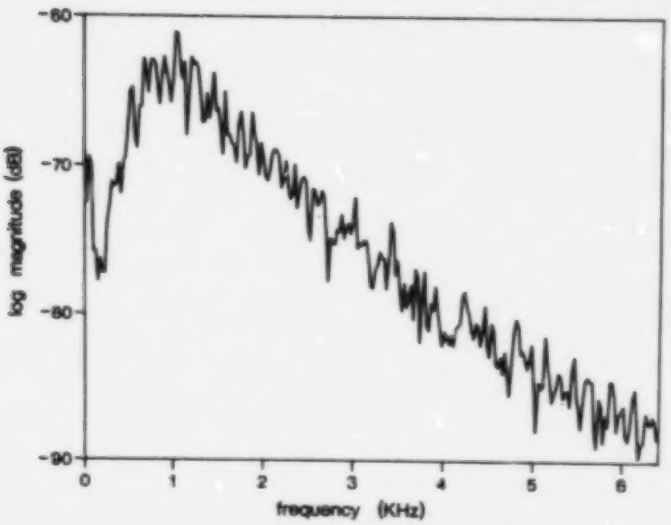

Fig. 8(a)

The average of 10 autospectra for the subclavian vein at rest with no bubbles.

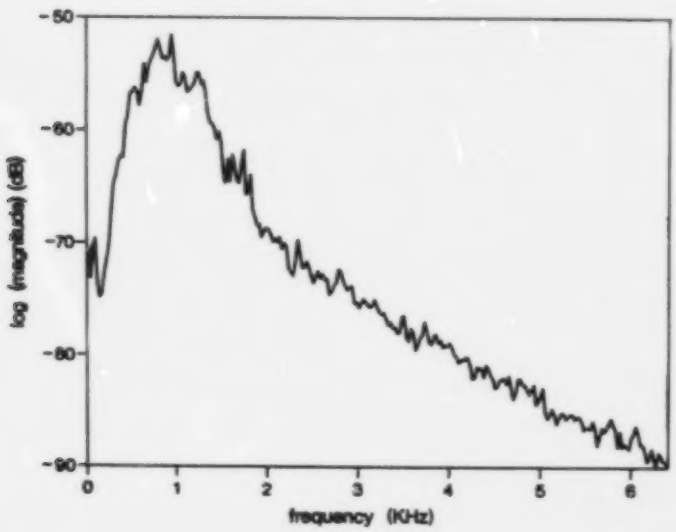

Fig. 8(b)

The average of 50 autospectra for the subclavian vein at rest when numerous bubbles (Grade III+) were present.

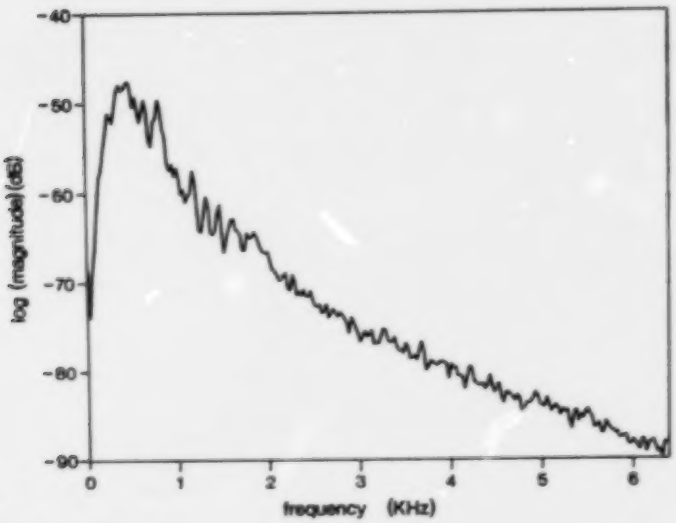

Fig. 9(a)

The average of 35 autospectra for the precordial signal for the second subject at rest.

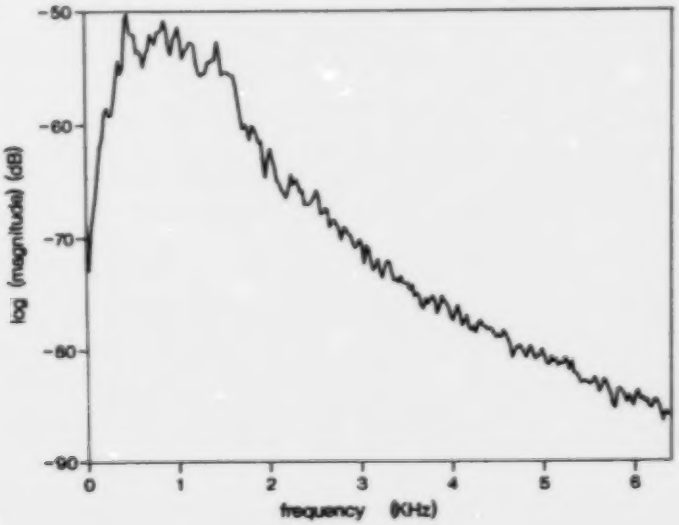

Fig. 9(b)

The average of 80 autospectra for the precordial signal for the second subject at rest, when many bubbles (Grade III) were detected.

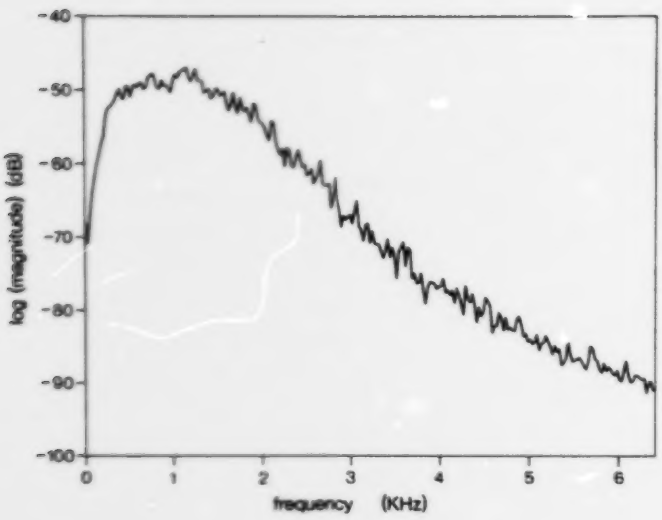

Fig. 9(c)

The average of 40 autospectra for the precordial signal for the second subject after movement, when a shower of bubbles (Grade IV) were detected.

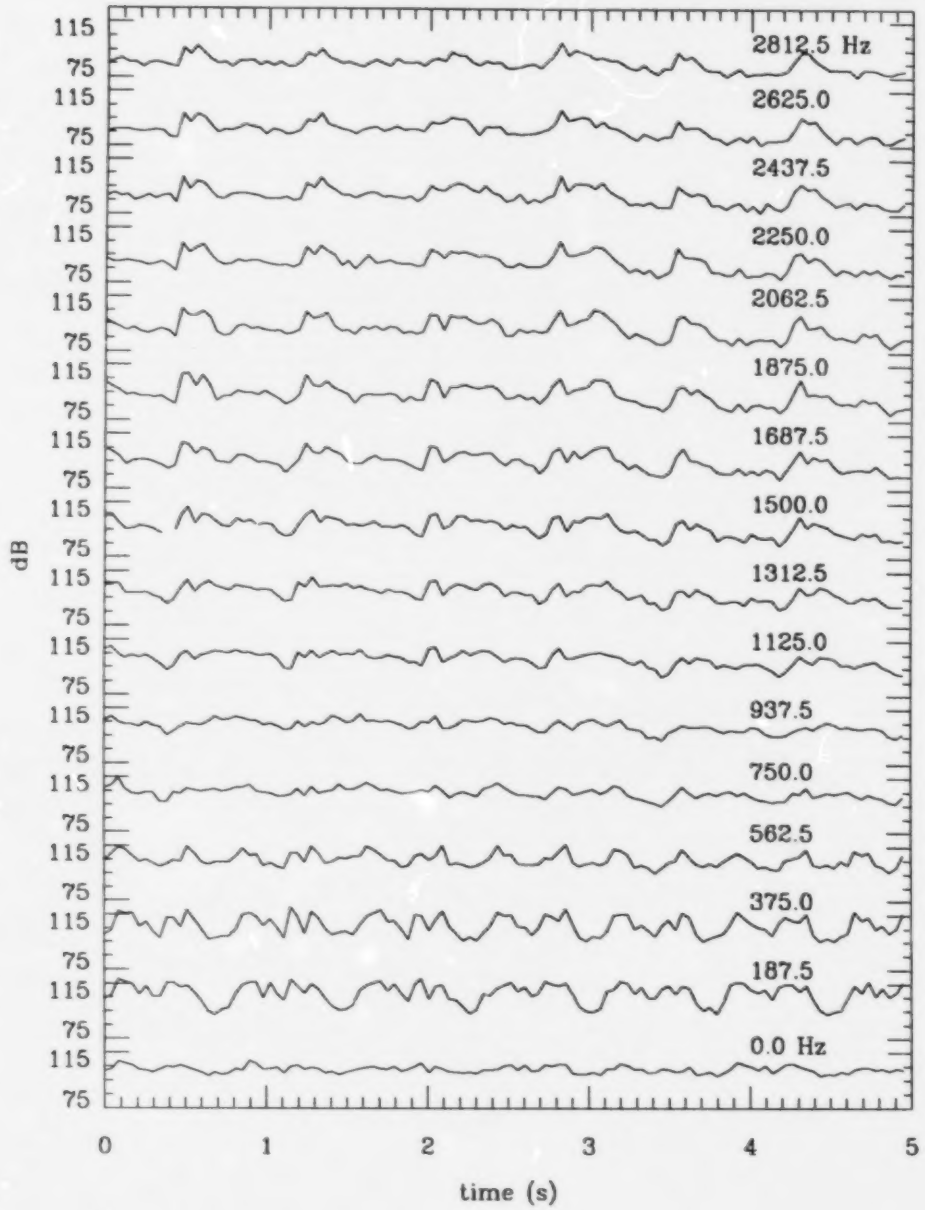

Fig. 10(a)

A spectrogram showing the logarithm of the magnitude of each of 16 spectral lines from 0 to 2812.5 Hz. The plot should be viewed as 16 separate plots, each on a scale from 75 to 115 dB. This spectrogram illustrates the reference precordial signal for the first subject, standing at rest. It has the lowest resolution in time; the window duration was 40 ms.

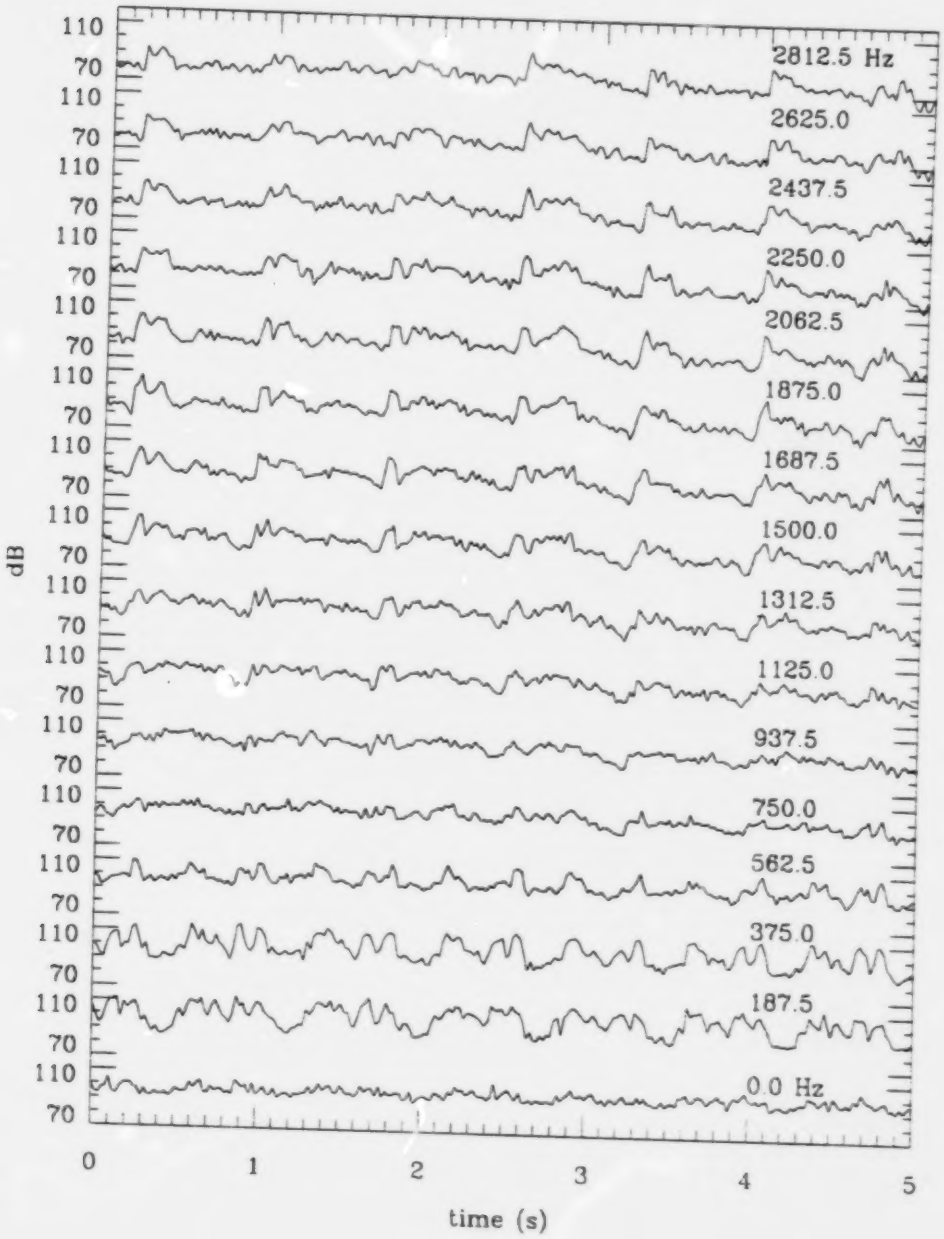

Fig. 10(b)

The spectrogram for the same signals as shown in part (a), but with the window duration shortened to 20 ms.

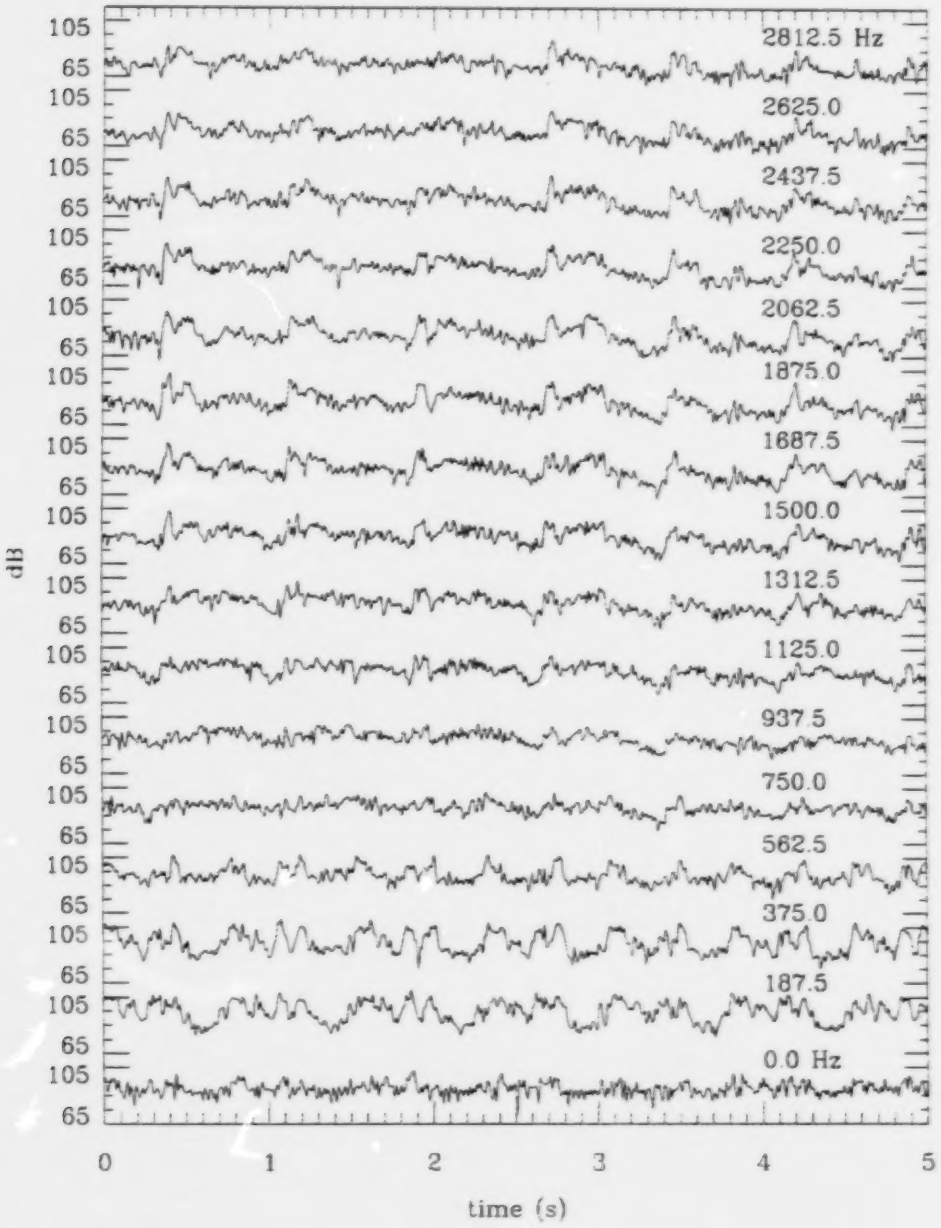

Fig. 10(c)

The spectrogram for the same signals as in parts (a) and (b), but with the window duration further shortened to 10 ms.

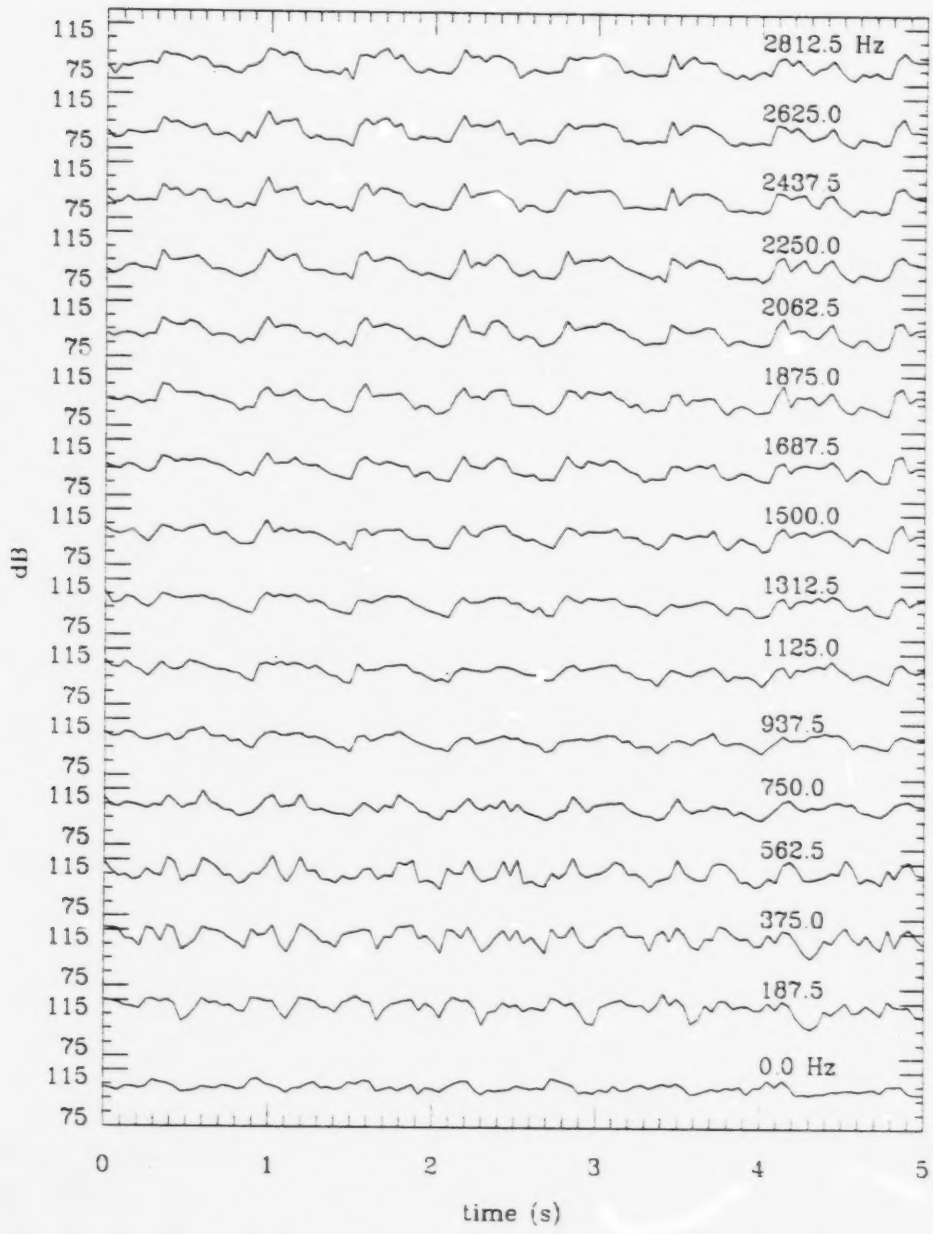

Fig. 10(d)

A specrtrogram, with a window duration of 40 ms, for the reference precordial signals for the first subject, after movement.

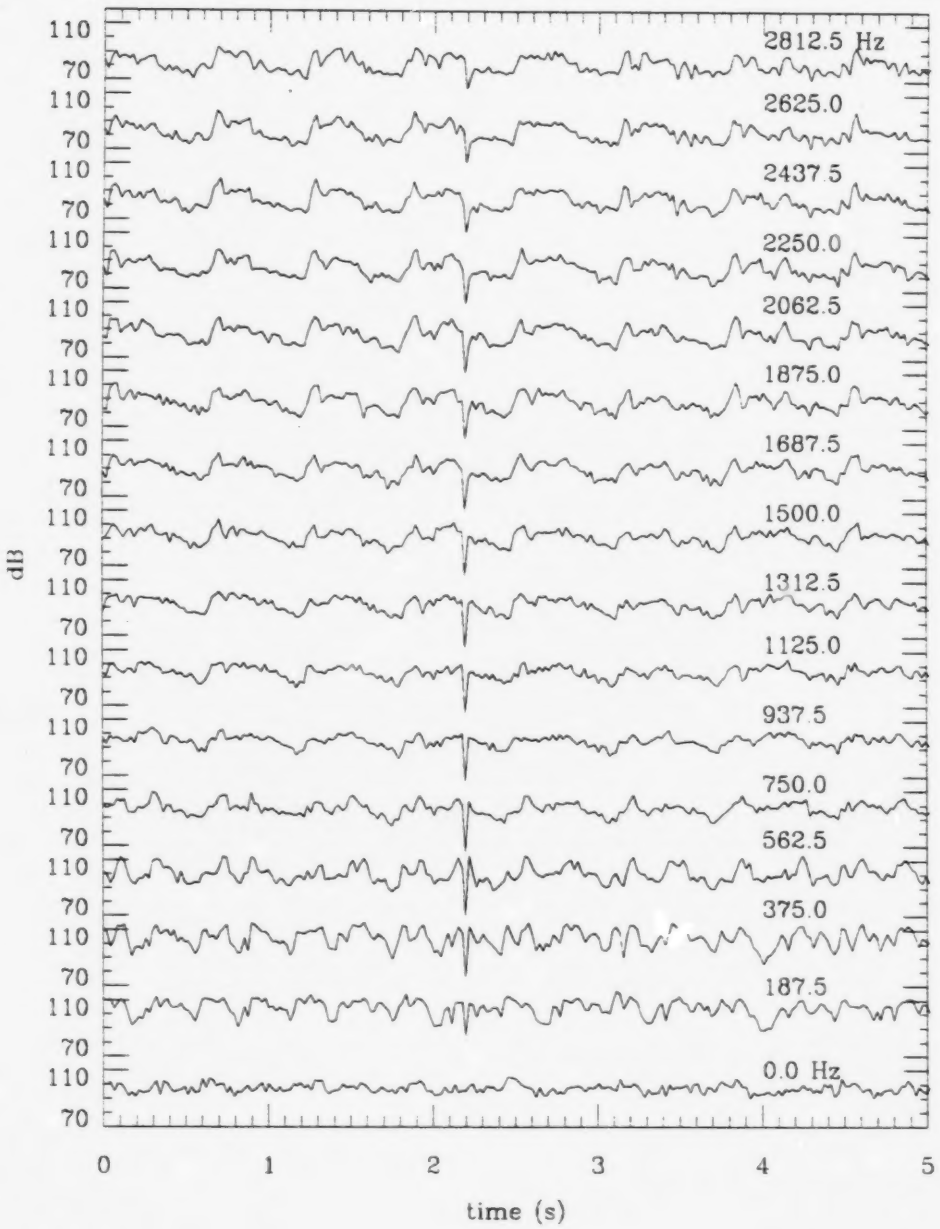

Fig. 10(e)

The spectrogram for the same signals as in part (d), but with a window duration of 20 ms. The deep trough at about 2.2s was likely caused by a tape drop-out.

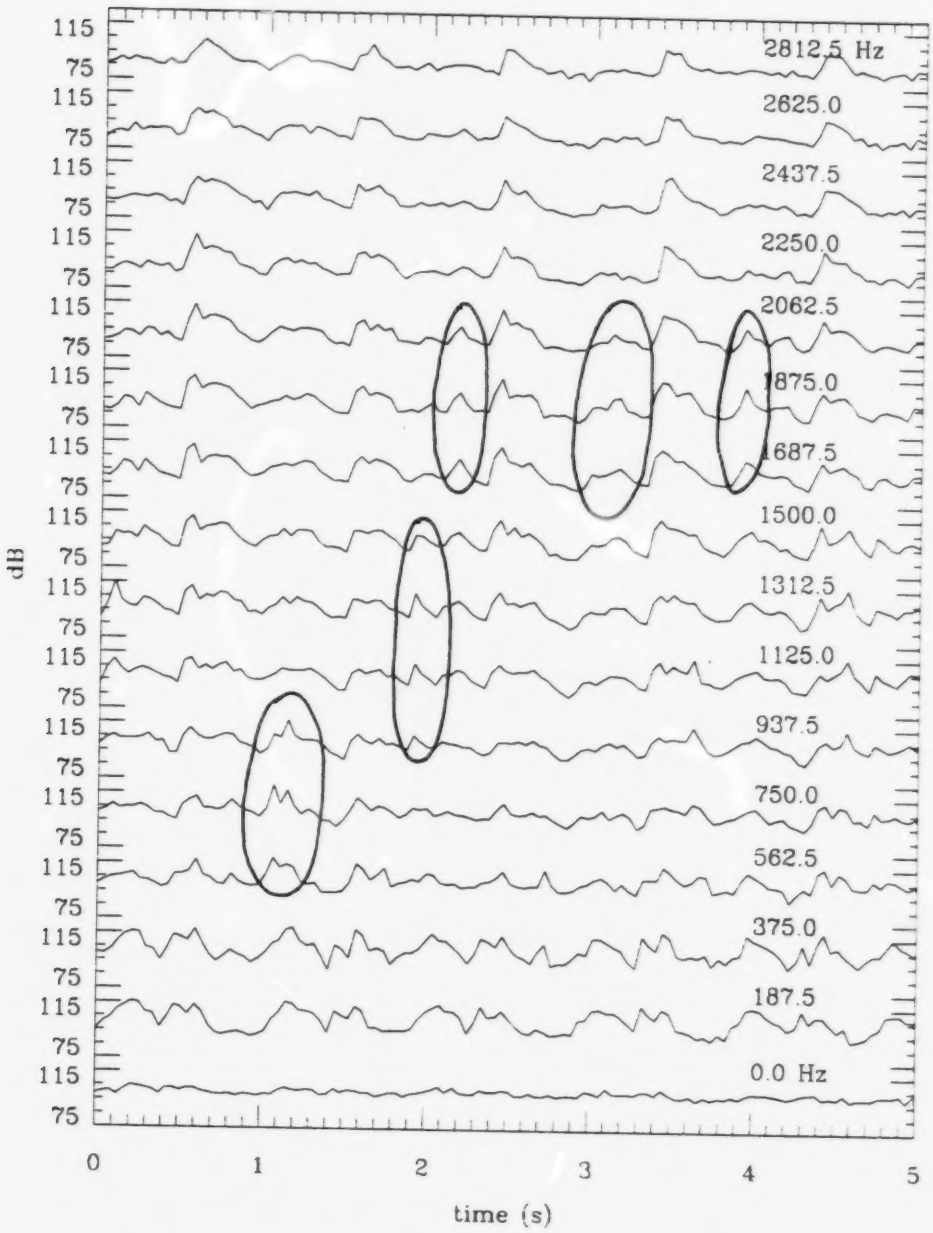

Fig. 11(a)

A spectrogram of the precordial signal from the first subject at rest, after a dive. The window duration was 40 ms. The extra peaks circled may be caused by transient signals from bubbles.

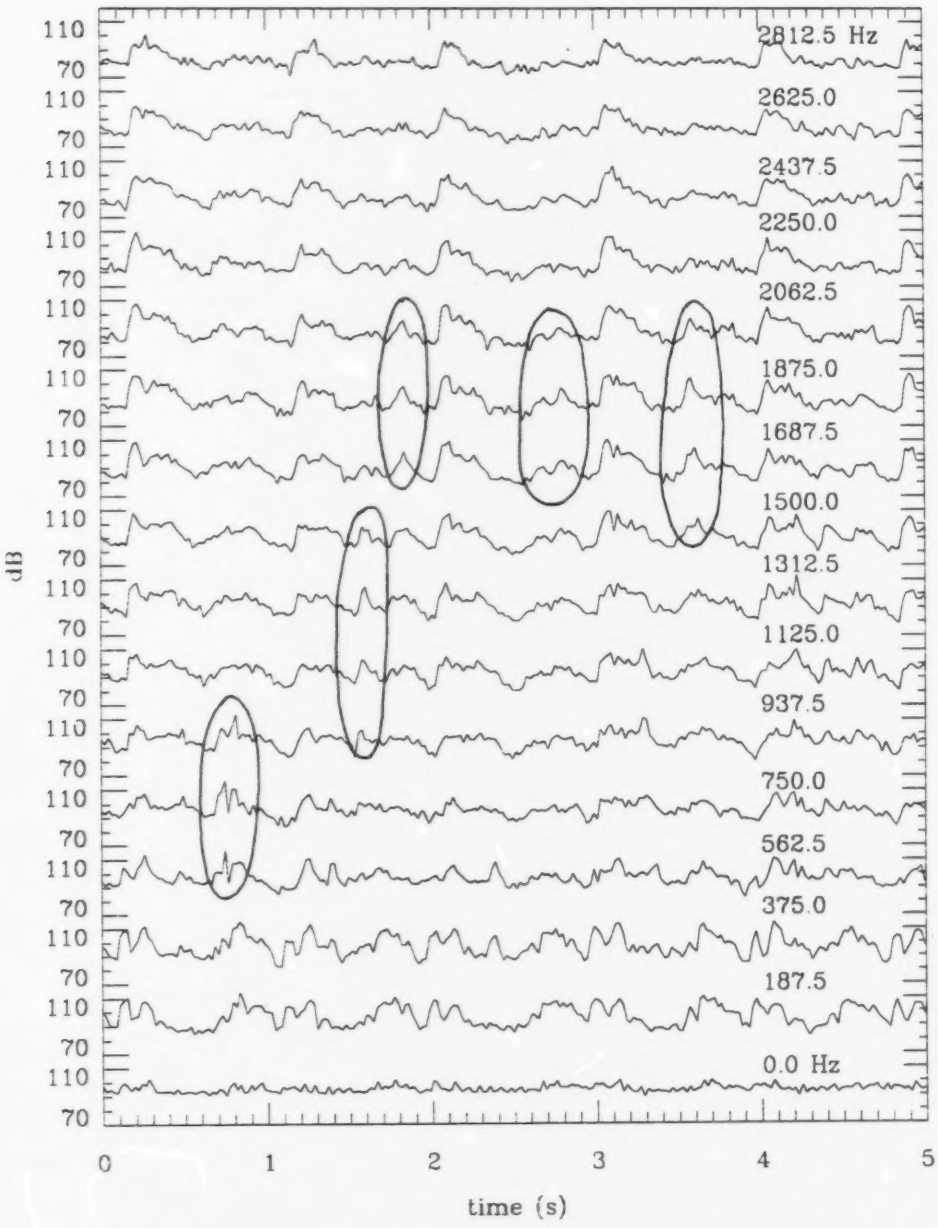

Fig. 11(b)

The spectrogram for the same signals as in part (a), but with a window duration of 20 ms.

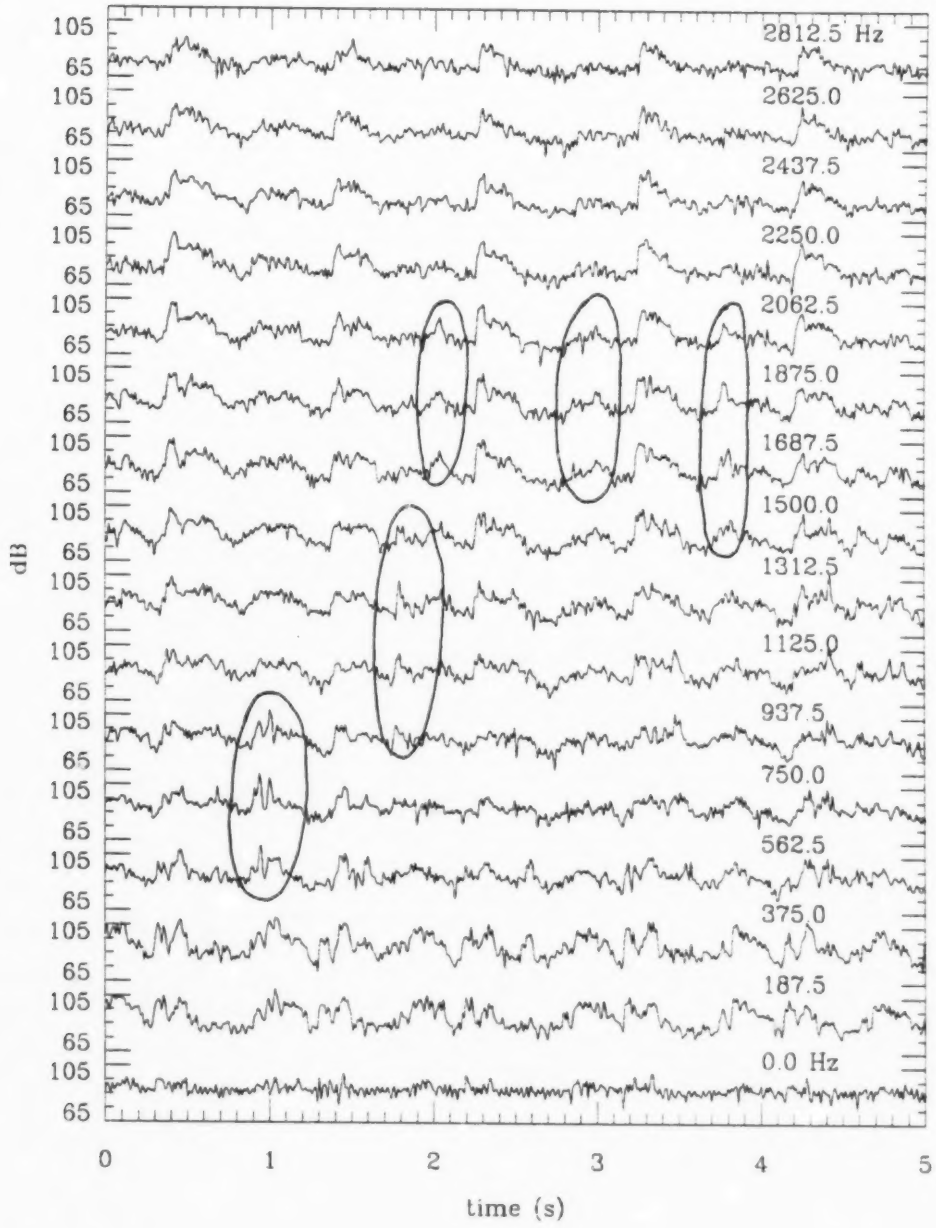

Fig. 11(c)
The spectrogram for the same signals as in part (a), but with a window duration of 10 ms.

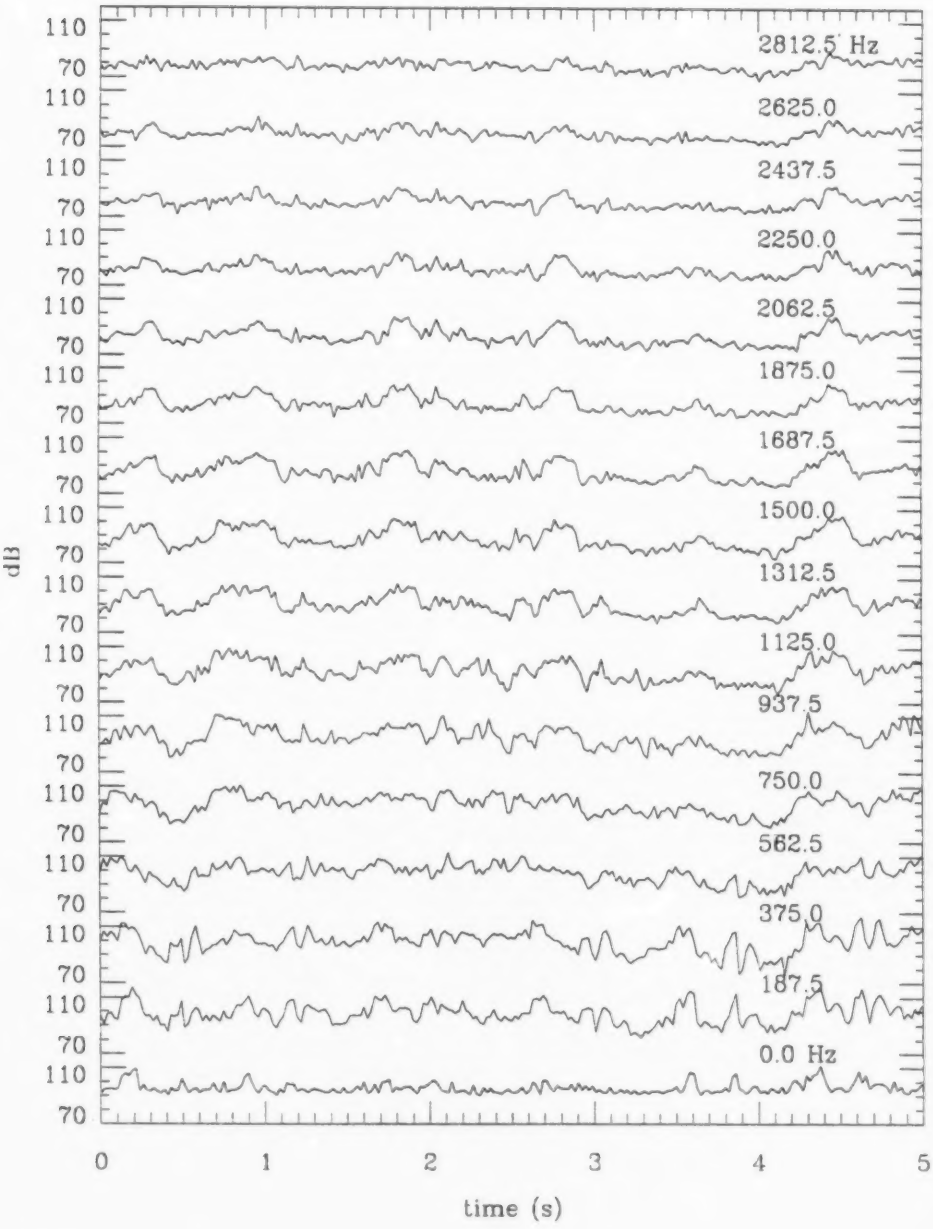

Fig. 11(d)

A spectrogram of the precordial signal from the first subject after movement, after decompression. The window duration was 20 ms. Many bubbles were present, and the bubble signals have begun to override the normal features of the spectrogram.

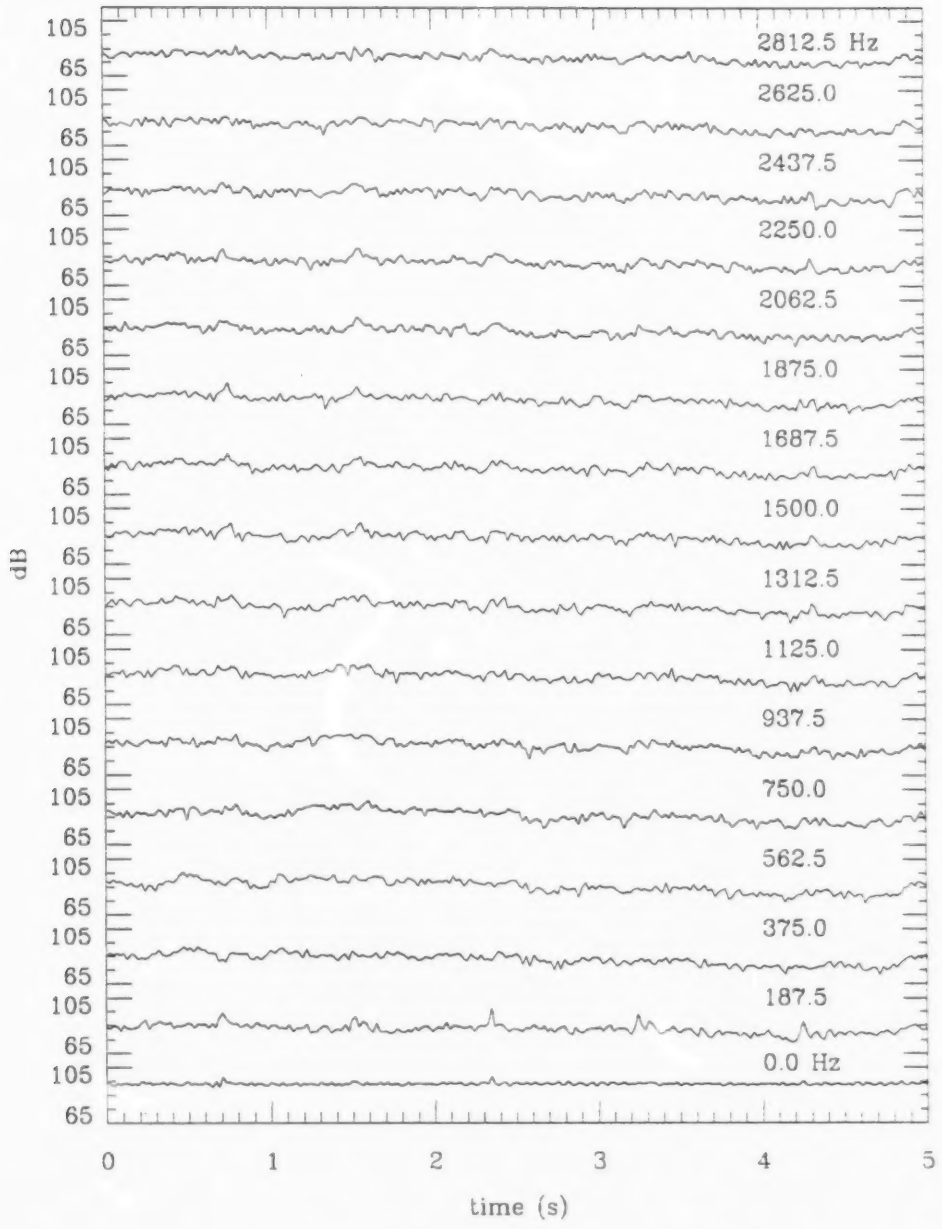

Fig. 12(a)

A spectrogram of the signal from a subclavian vein of the first subject, when no bubbles were present. The window duration was 20 ms.

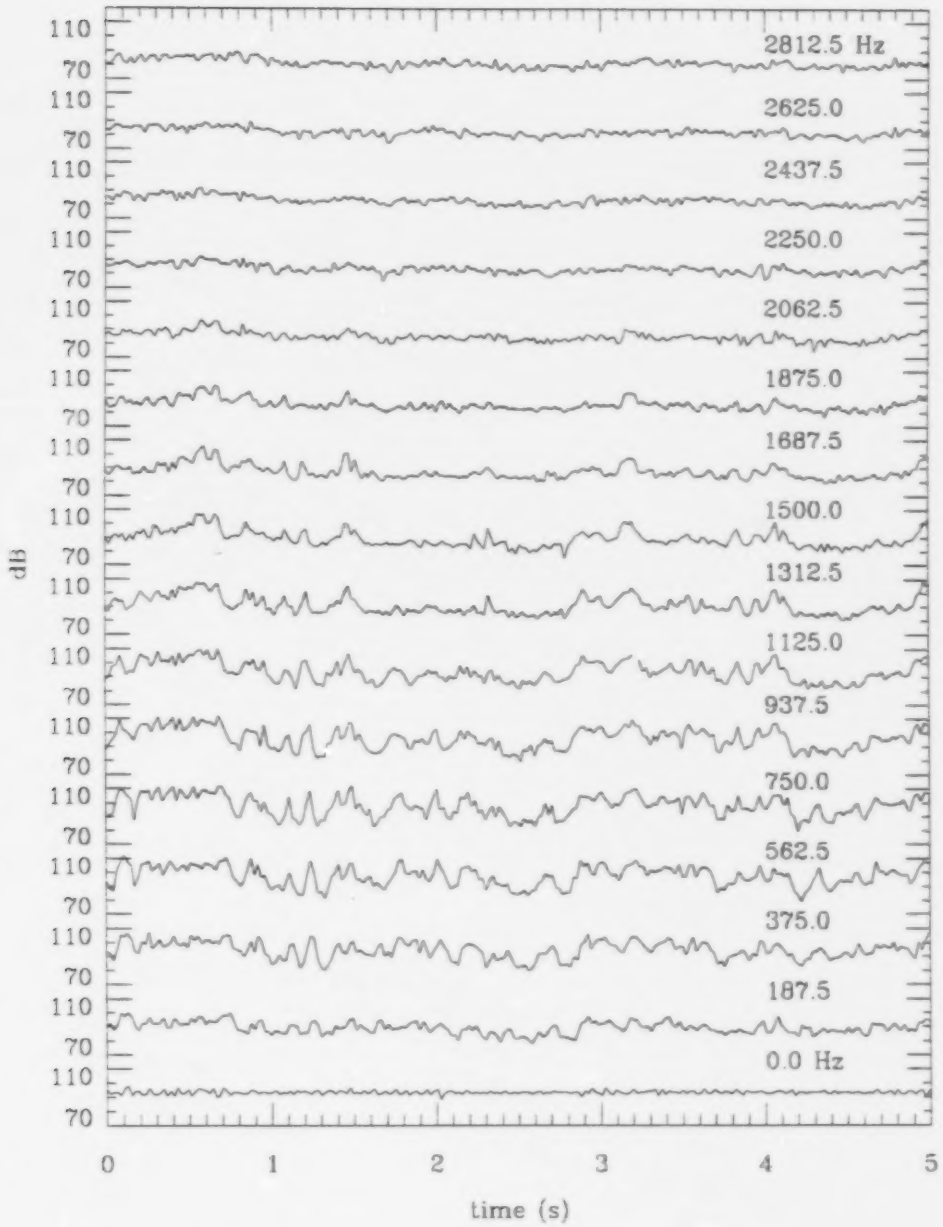

Fig. 12(b)

A spectrogram of the signal from a subclavian vein of the first subject, when numerous bubbles were present. The window duration was 20 ms.

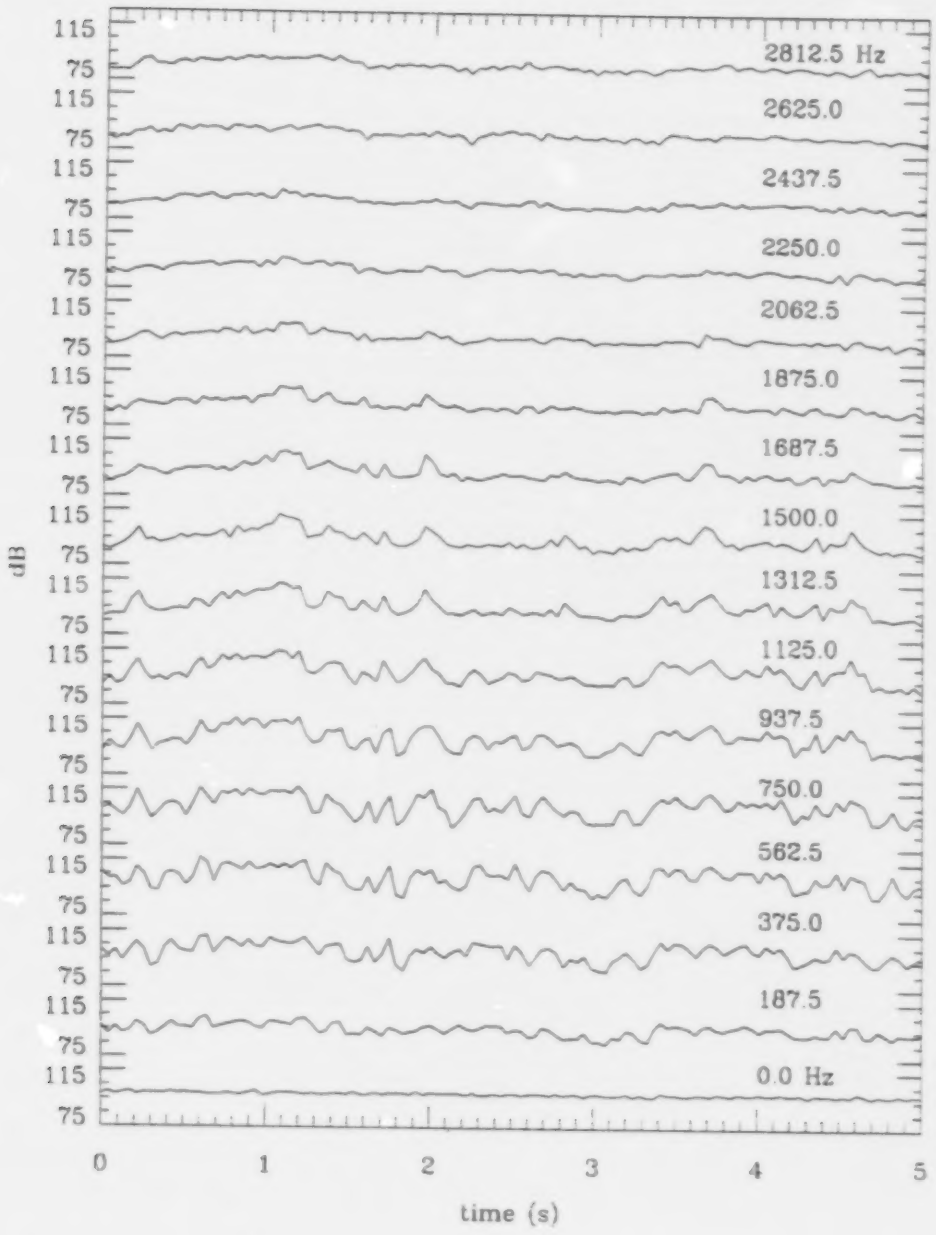

Fig. 12(c)

The spectrogram for the same signals as in part (b), but with a window duration of 40 ms. The bubble signals are not as well resolved in this case.

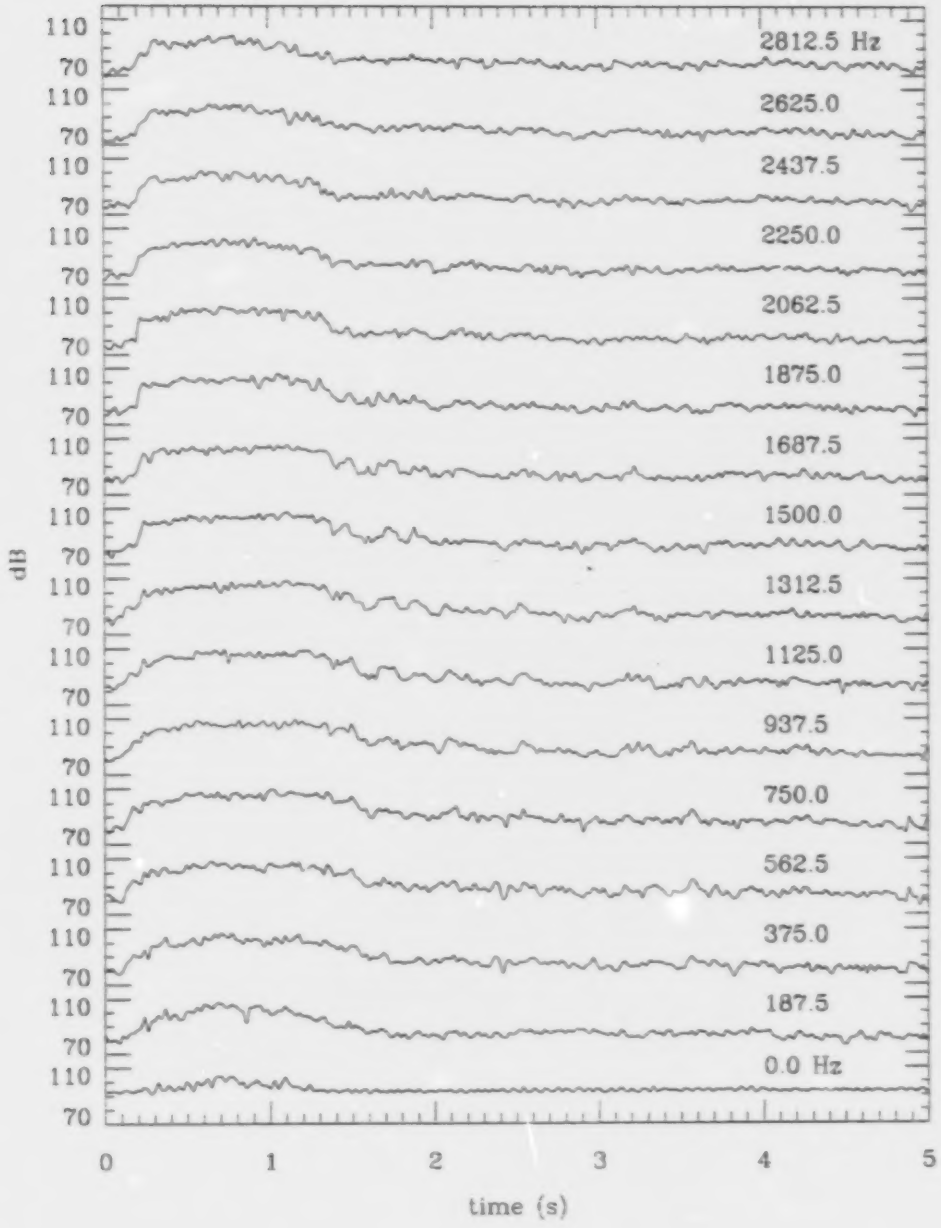

Fig. 12(d)
The spectrogram after the subject clenched his fist, causing a brief shower of bubbles. The window duration was 20 ms.

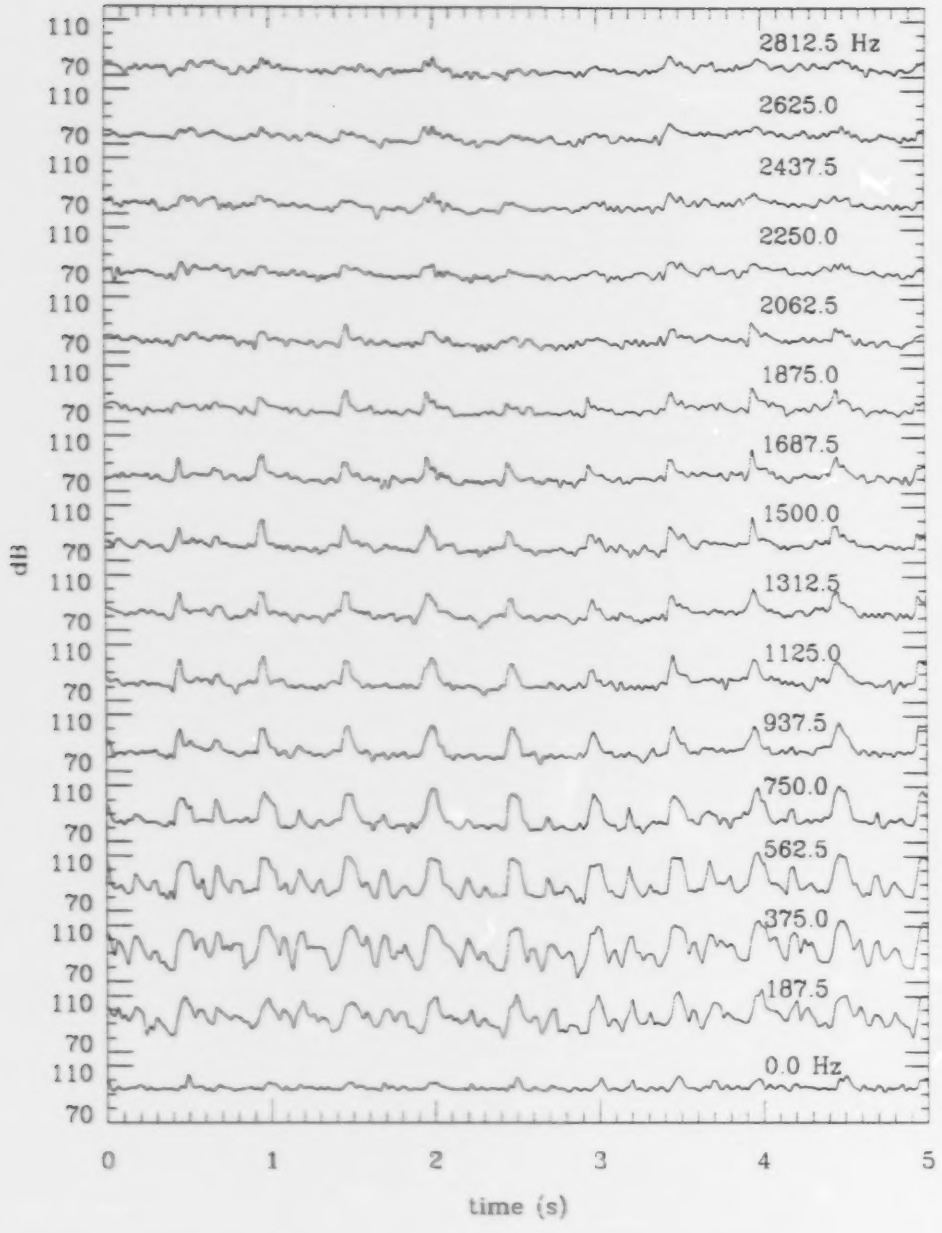

Fig. 13(a)

A spectrogram of the reference precordial signal from the second subject at rest. The window duration was 20 ms.

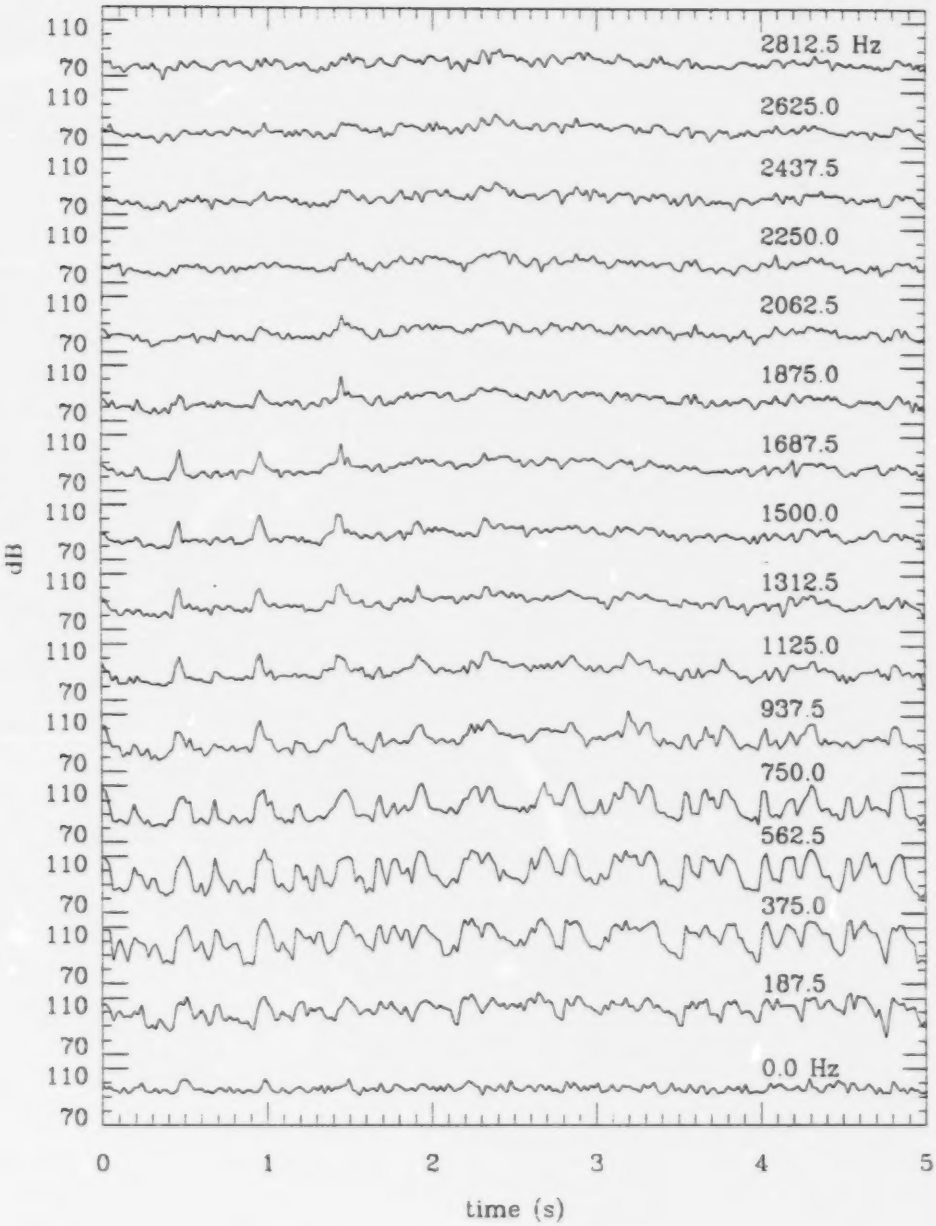

Fig. 13(b)

A spectrogram of the reference precordial signal from the second subject after movement.

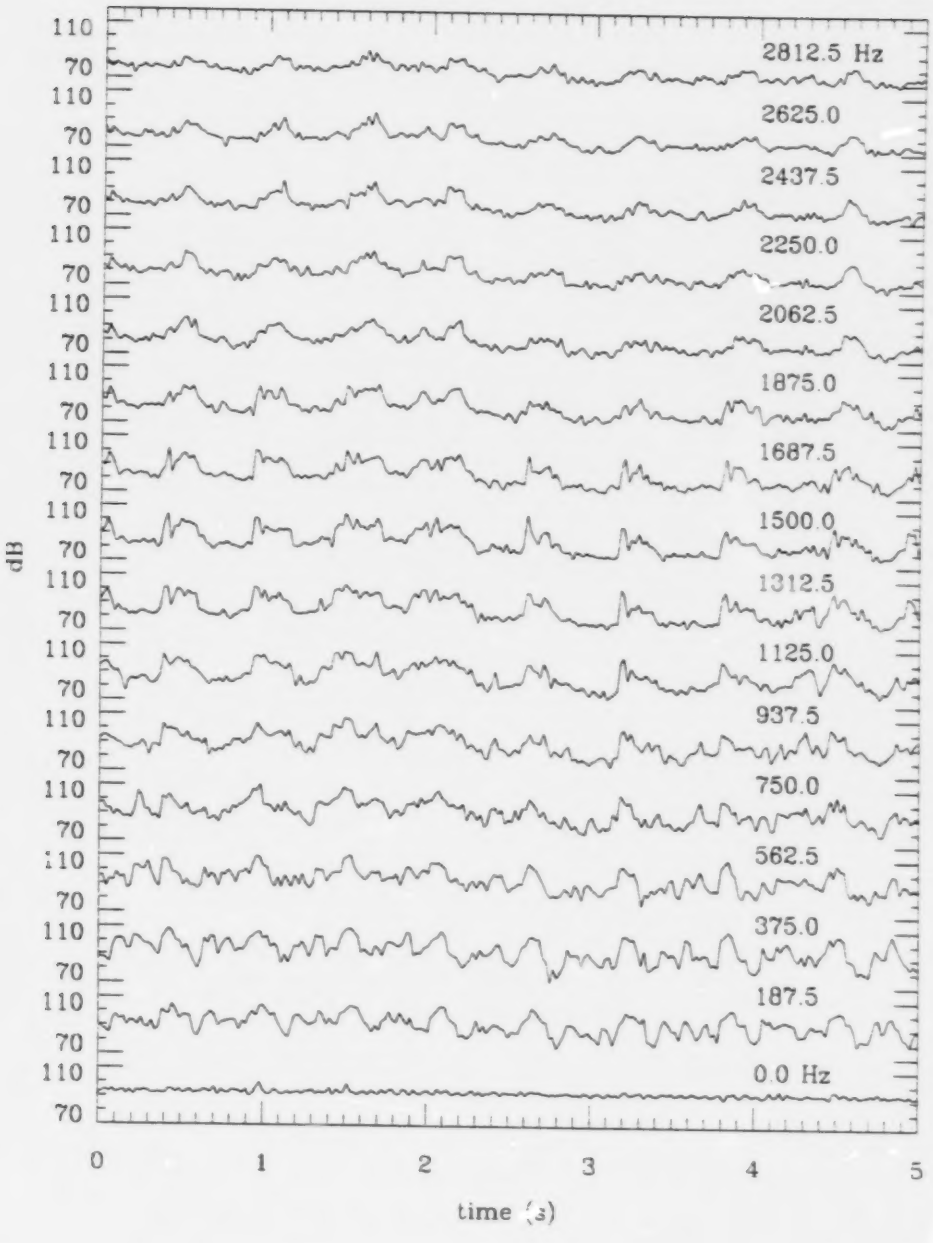

Fig. 13(c)

A spectrogram of the precordial signal from the second subject at rest after decompression, when many bubbles were present.

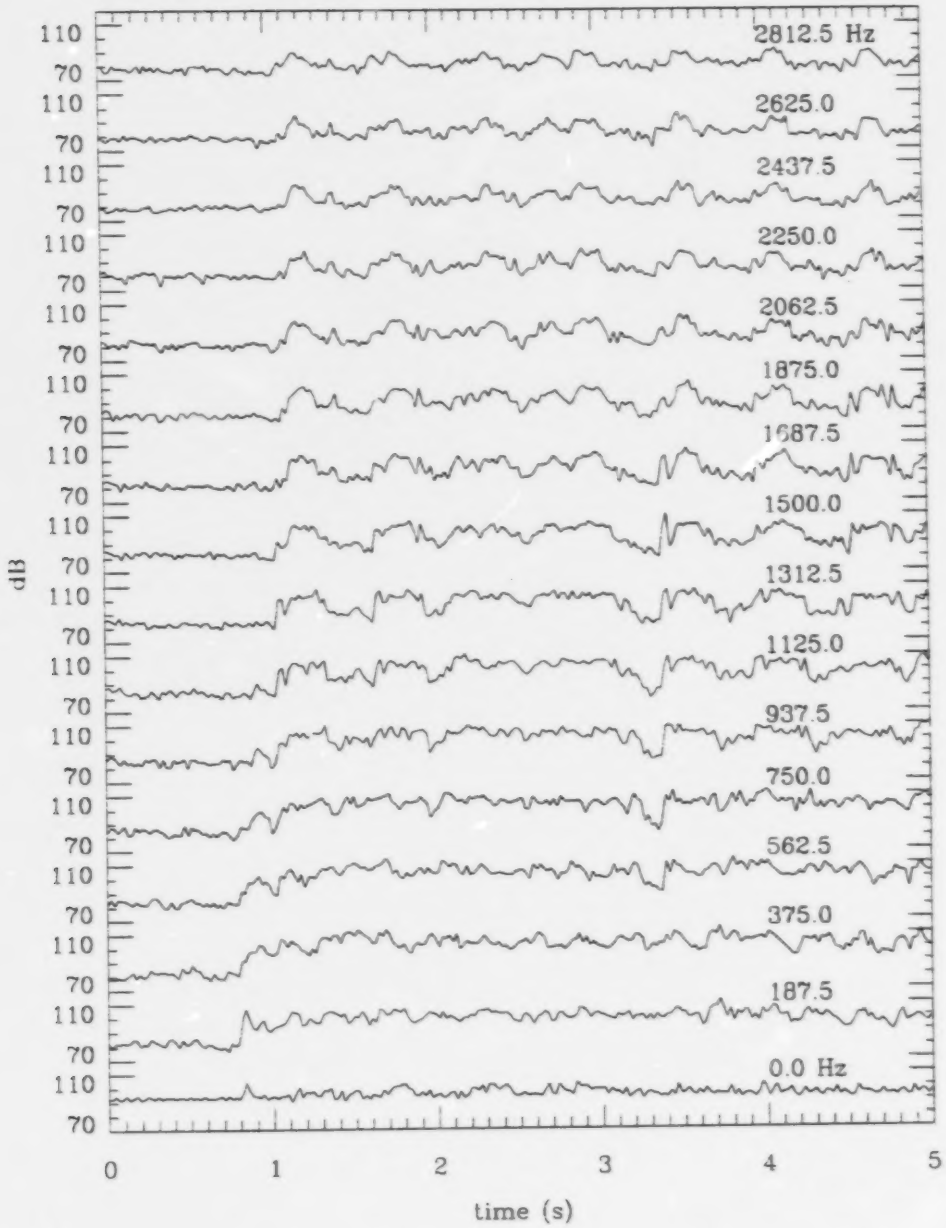

Fig. 13(d)

A spectrogram of the precordial signal after the second subject moved, provoking a shower of bubbles. The bubble signals obscure the normal cardiac signals.

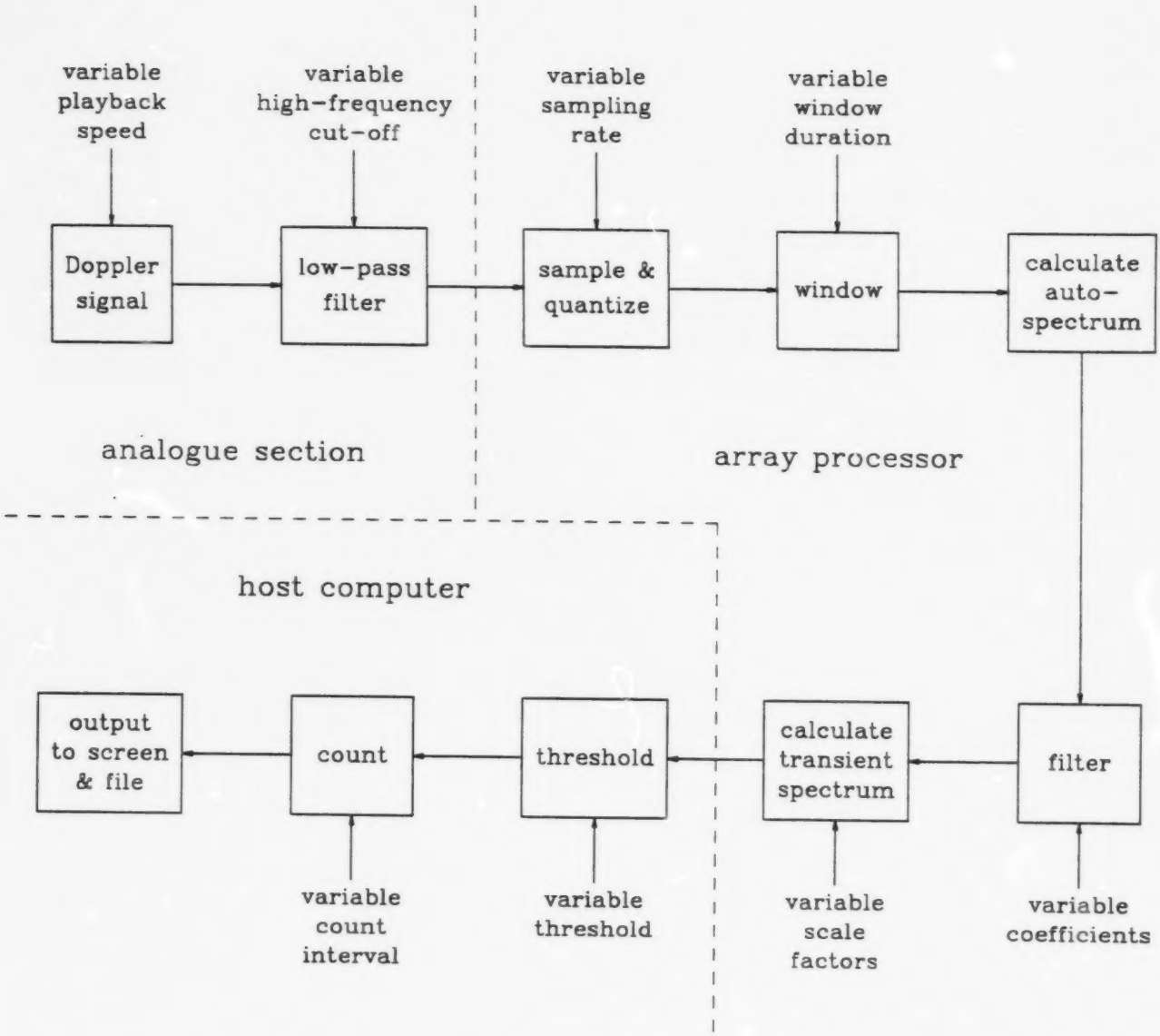

Fig. 14

A block diagram showing the steps in the bubble counting algorithm, and where they are carried out.

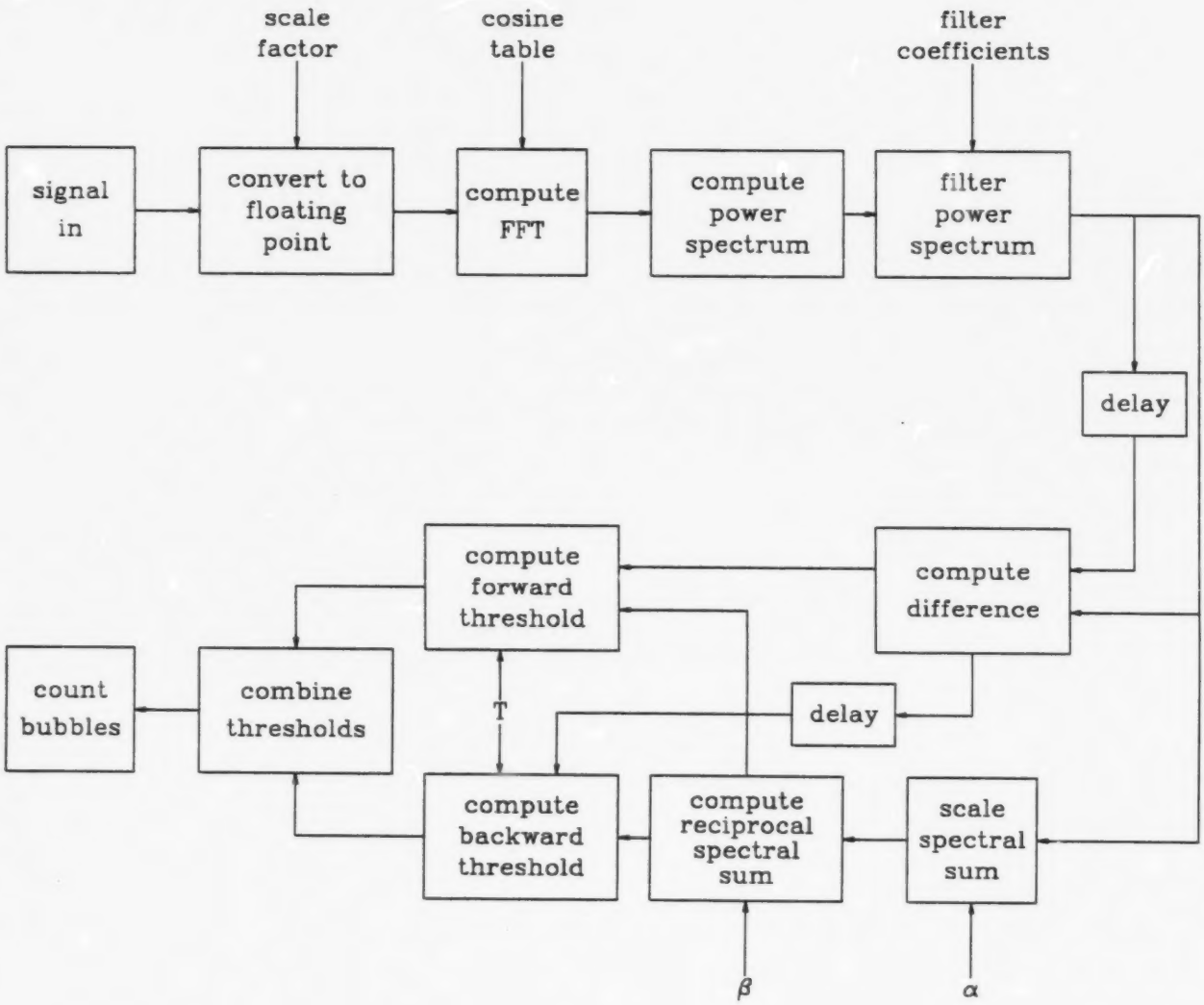

Fig. 15

A block diagram showing the steps of the algorithm in greater detail.

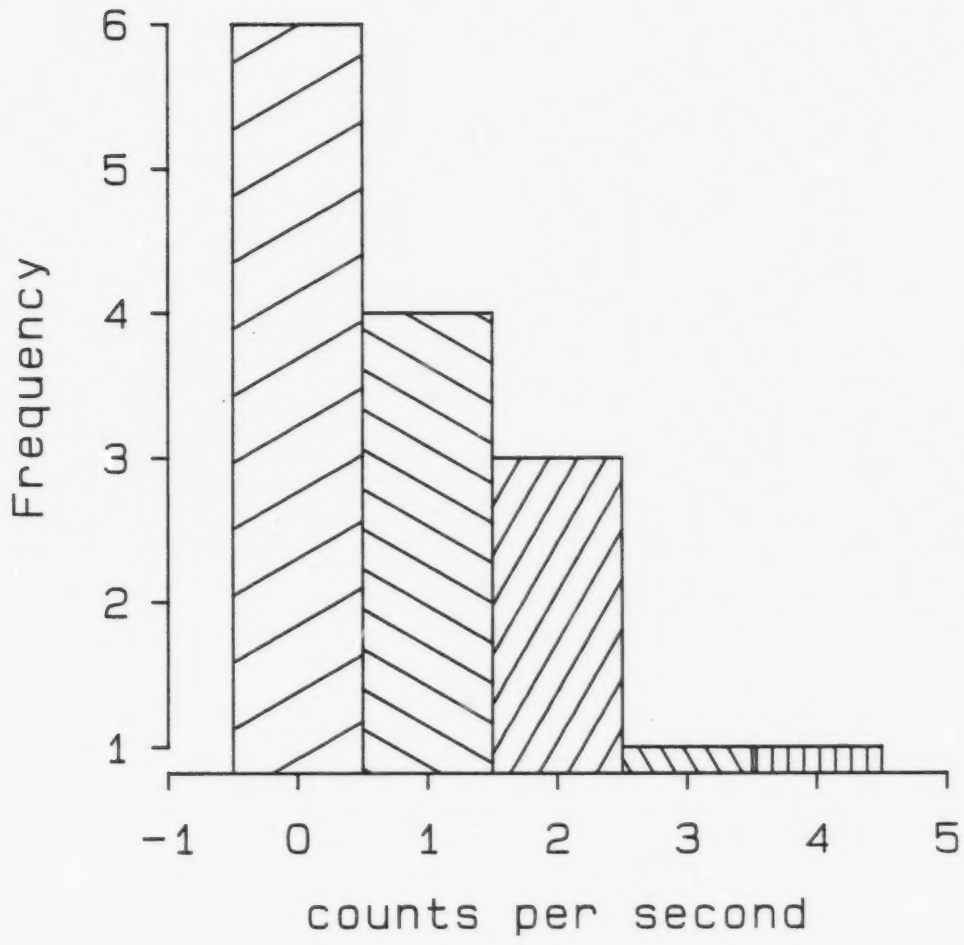

Fig. 16

A histogram of counts for the reference precordial signal for the first subject at rest.

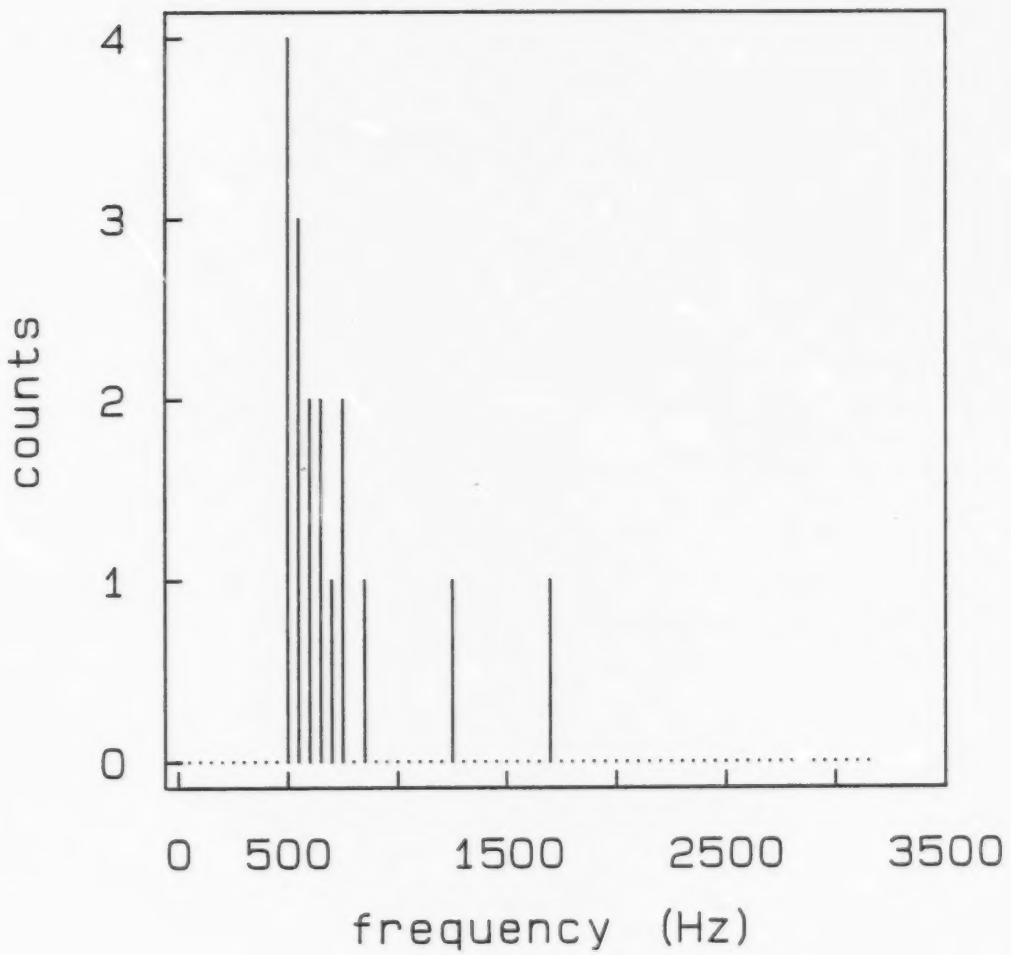

Fig. 17

A spectrogram showing the distribution of counts vs. frequency for the reference precordial signal of the first subject at rest.

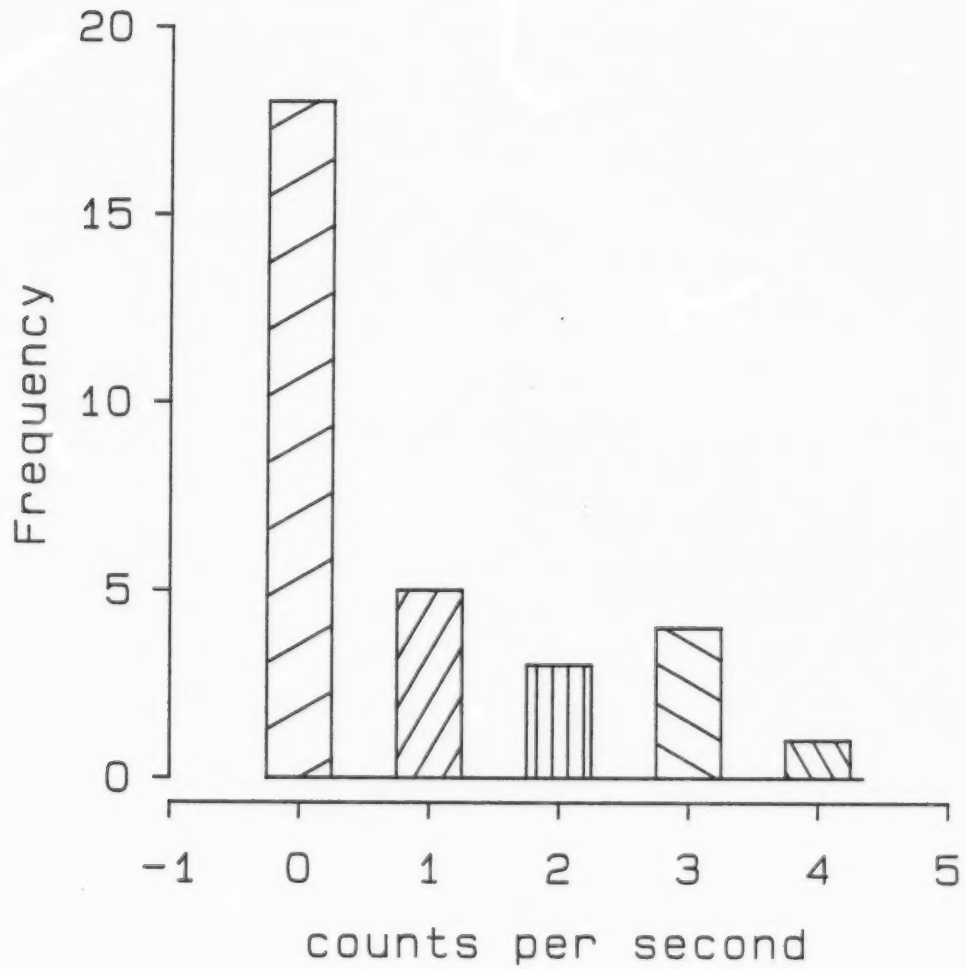

Fig. 18

A histogram of counts for the reference precordial signal for the first subject after movement.

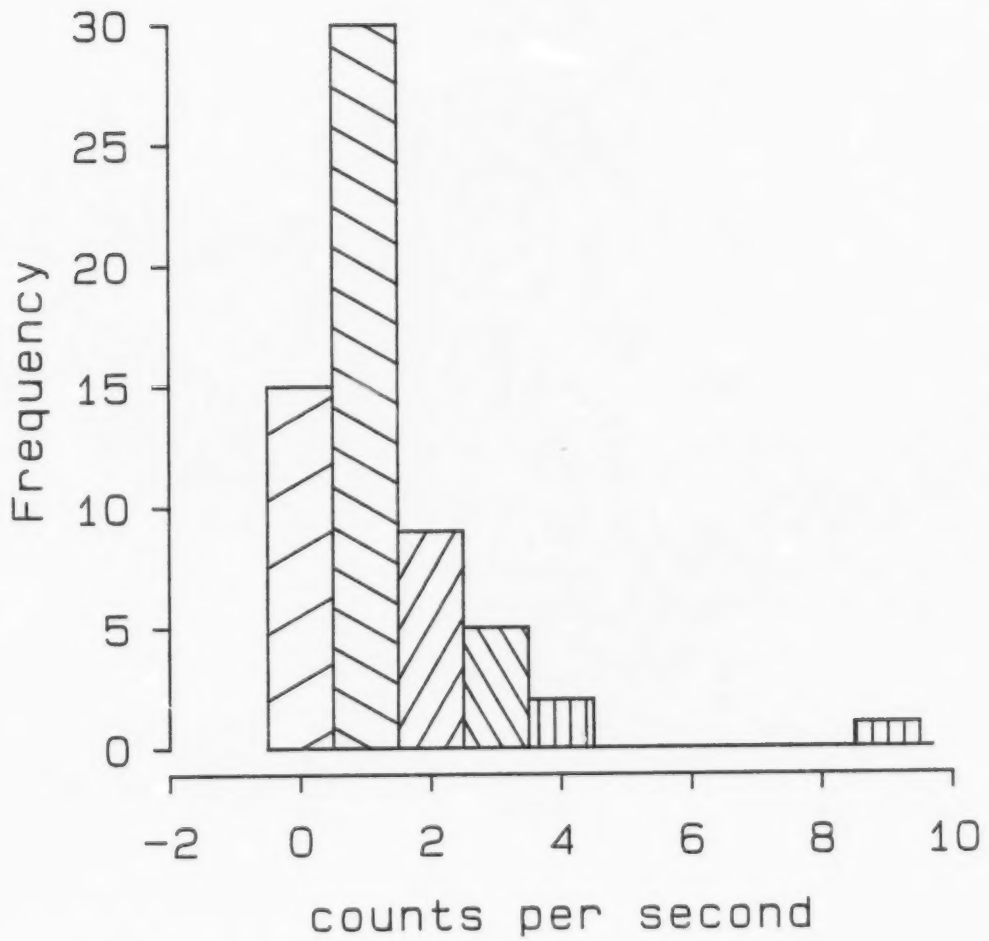

Fig. 19

A histogram of counts for the precordial signal of the first subject at rest. The observers classified the signal as Grade III- (KM Code 232).

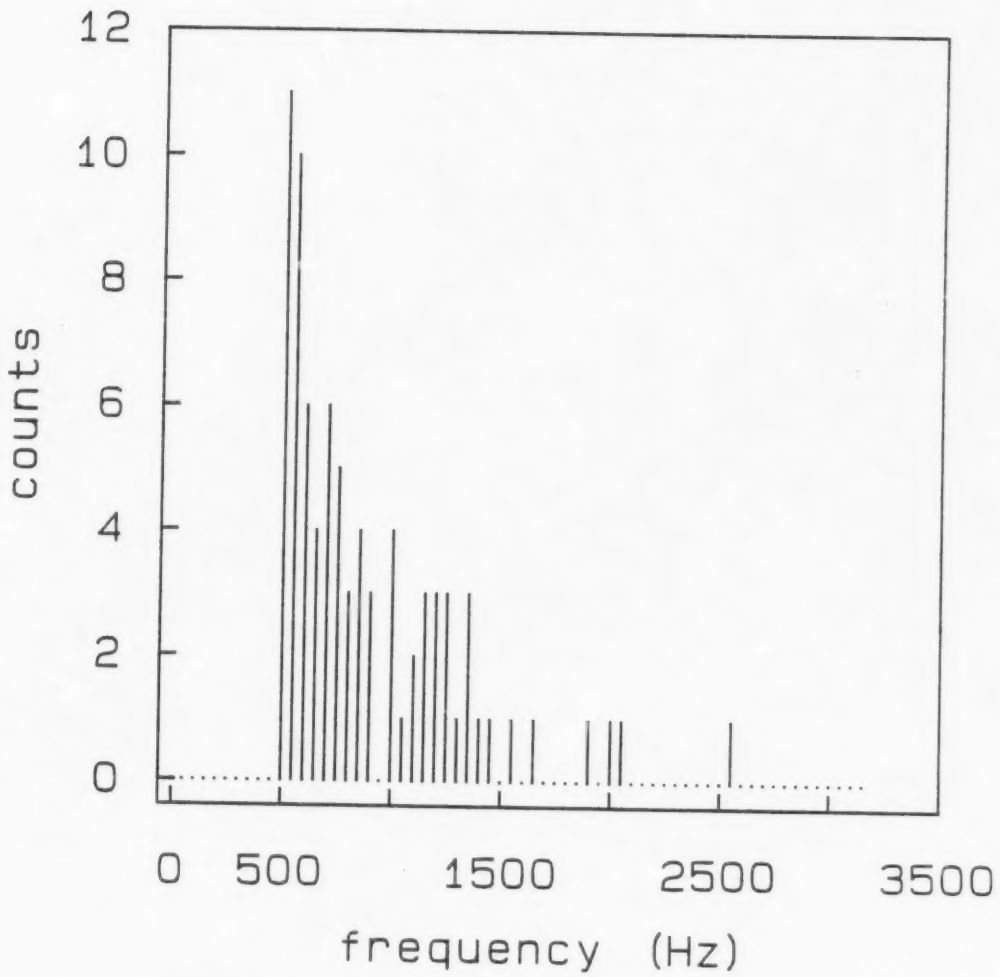

Fig. 20

A spectrogram showing the distribution of counts vs. frequency for the precordial signal of the first subject at rest. The signal was classified as Grade III- (KM Code 232).

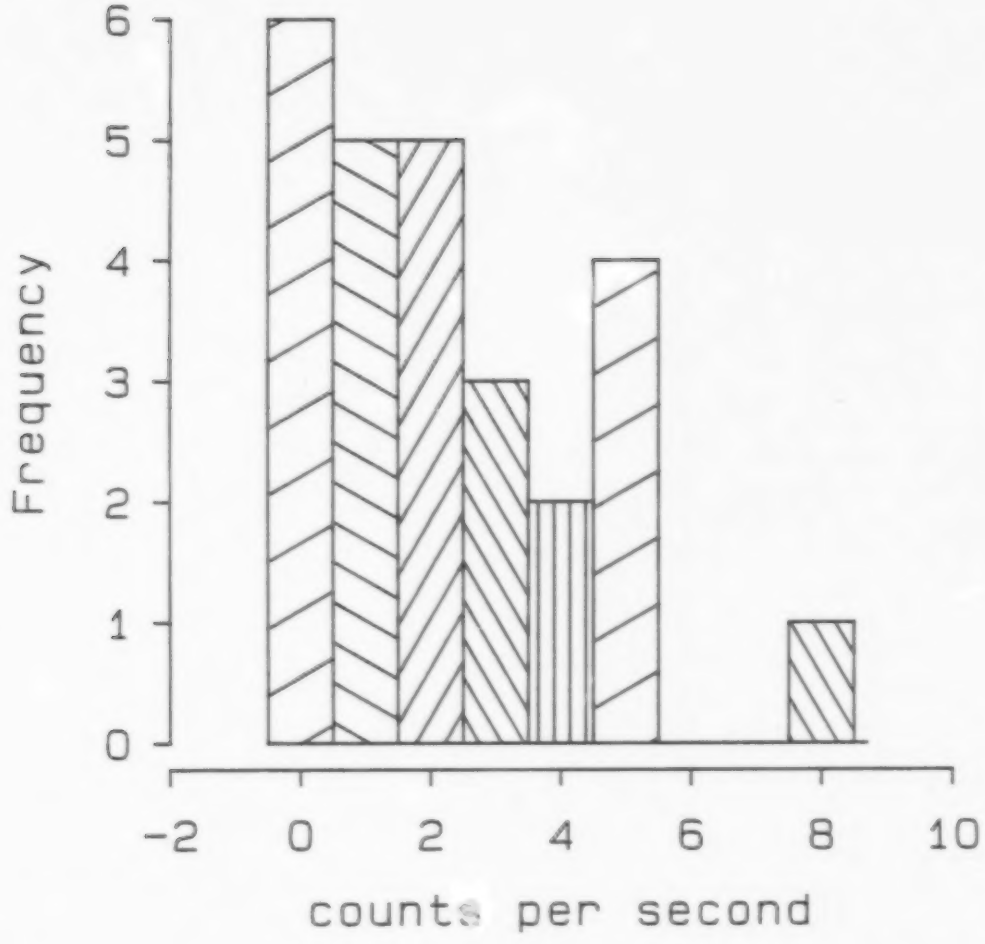

Fig. 21

A histogram of counts for the precordial signal of the first subject after movement. The signal was classified as Grade III+ (KM Code 343).

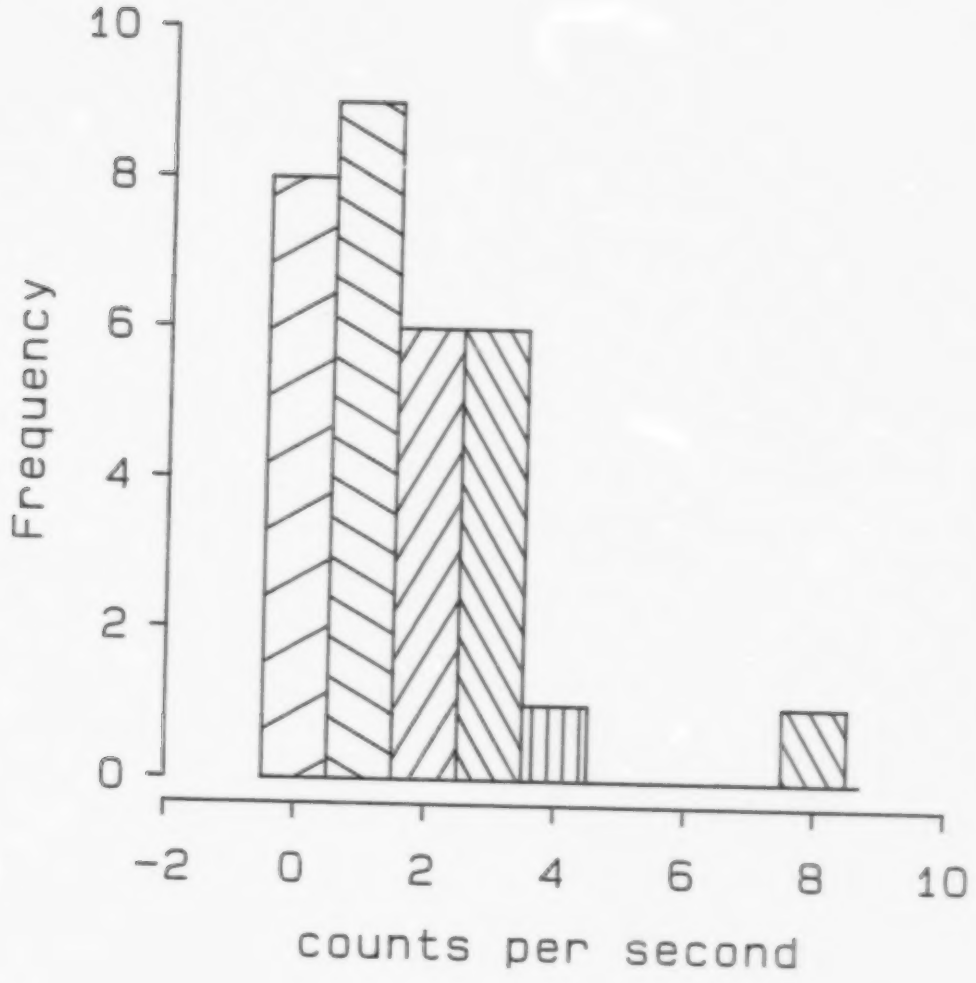

Fig. 22

A histogram of counts for a subclavian signal of the first subject at rest. The signal was classified as Grade III+ (KM Code 342).

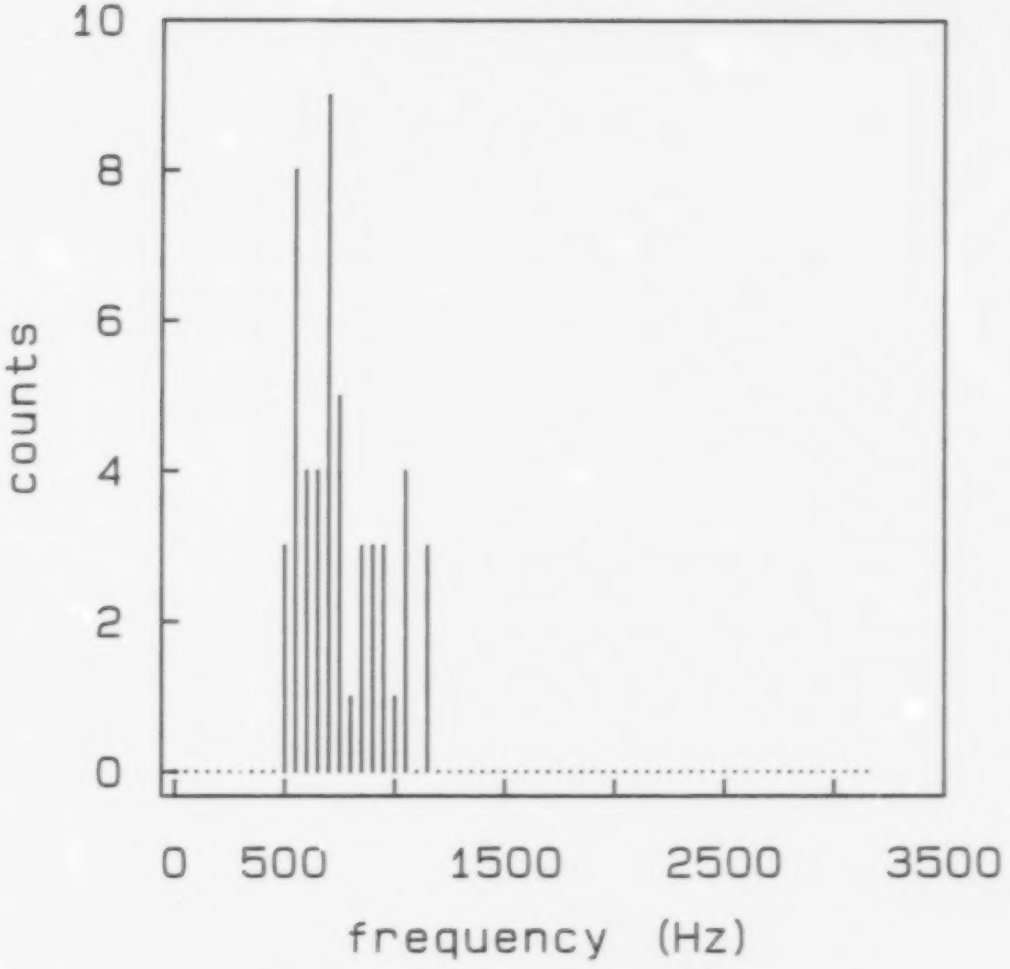

Fig. 23

A spectrogram showing the distribution of counts vs. frequency for a subcavian signal of the first subject at rest. The signal was classified as Grade III+ (KM Code 342).

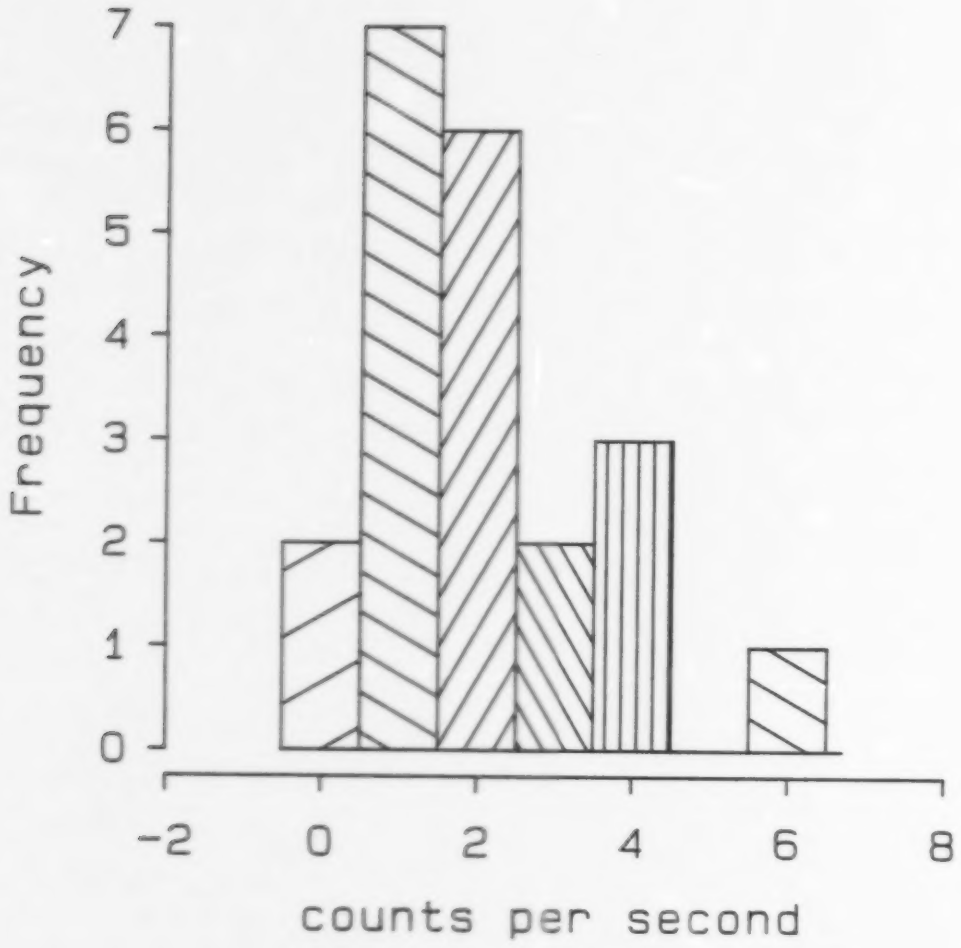

Fig. 24

A histogram of counts for the reference precordial signal for the second subject at rest.

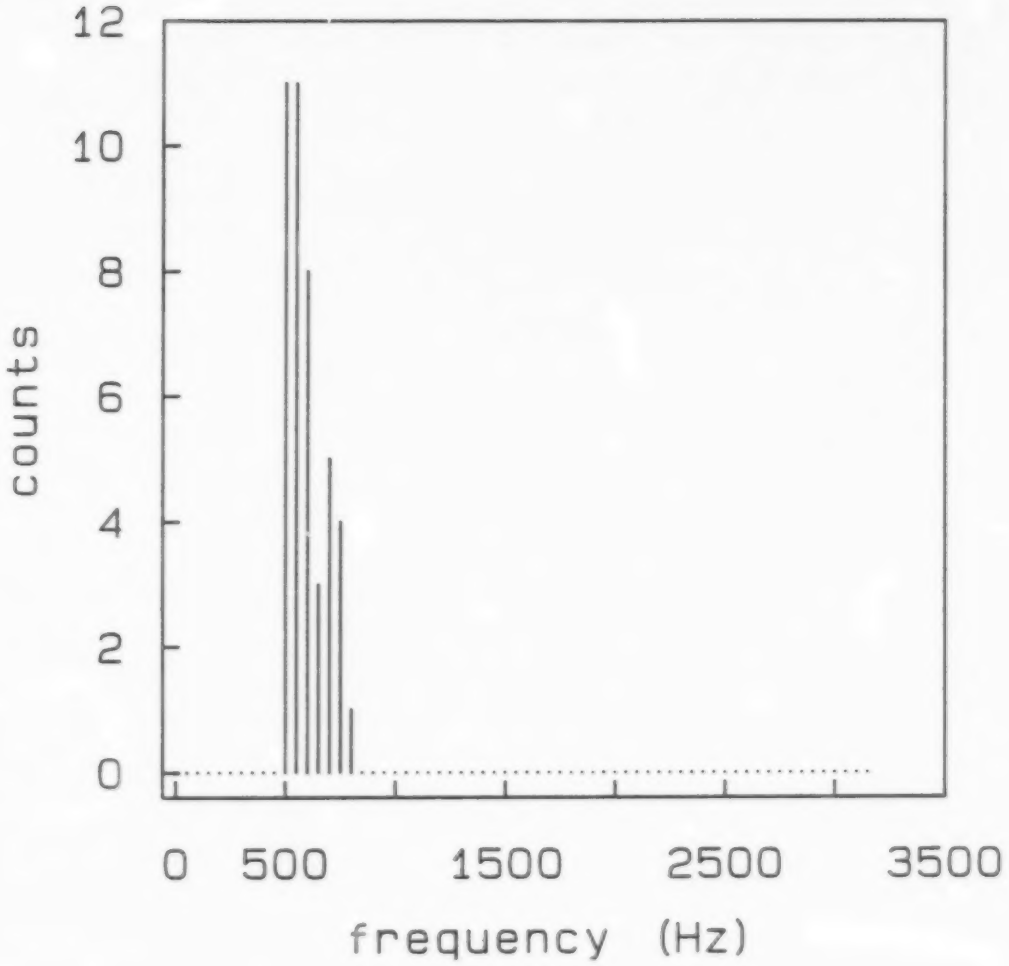

Fig. 25

A spectrogram showing the distribution of counts vs. frequency for the reference precordial signal of the second subject at rest.

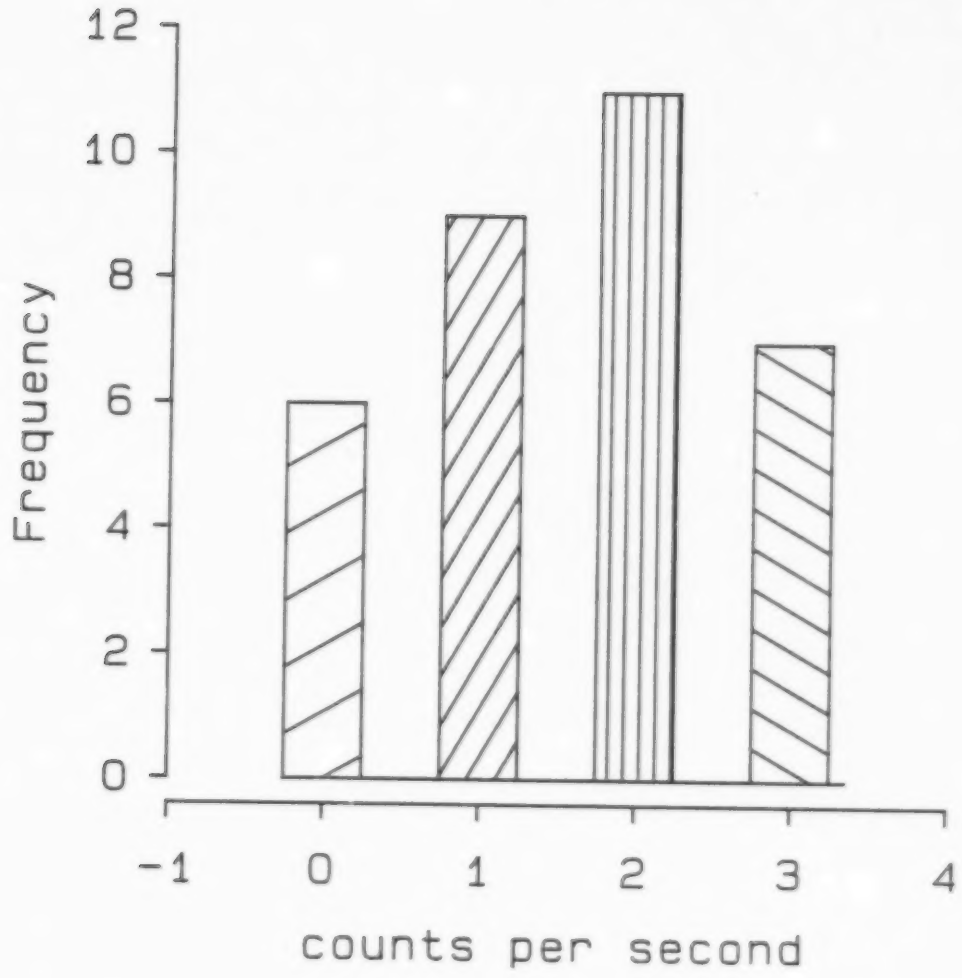

Fig. 26

A histogram of counts for the precordial signal of the second subject at rest. The signal was classified as Grade III (KM Code 243).

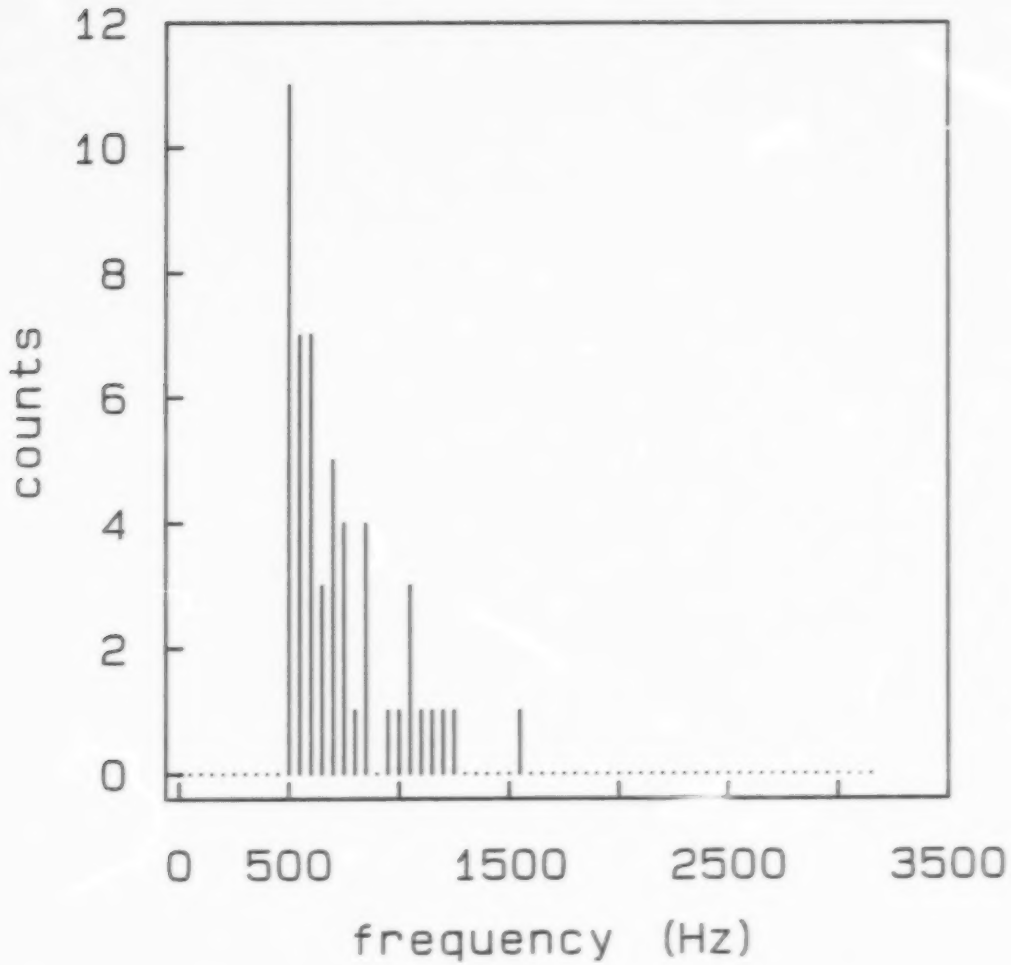

Fig. 27

A spectrogram showing the distribution of counts vs. frequency for the precordial signal of the second subject at rest. The signal was classified as Grade III (KM Code 243).

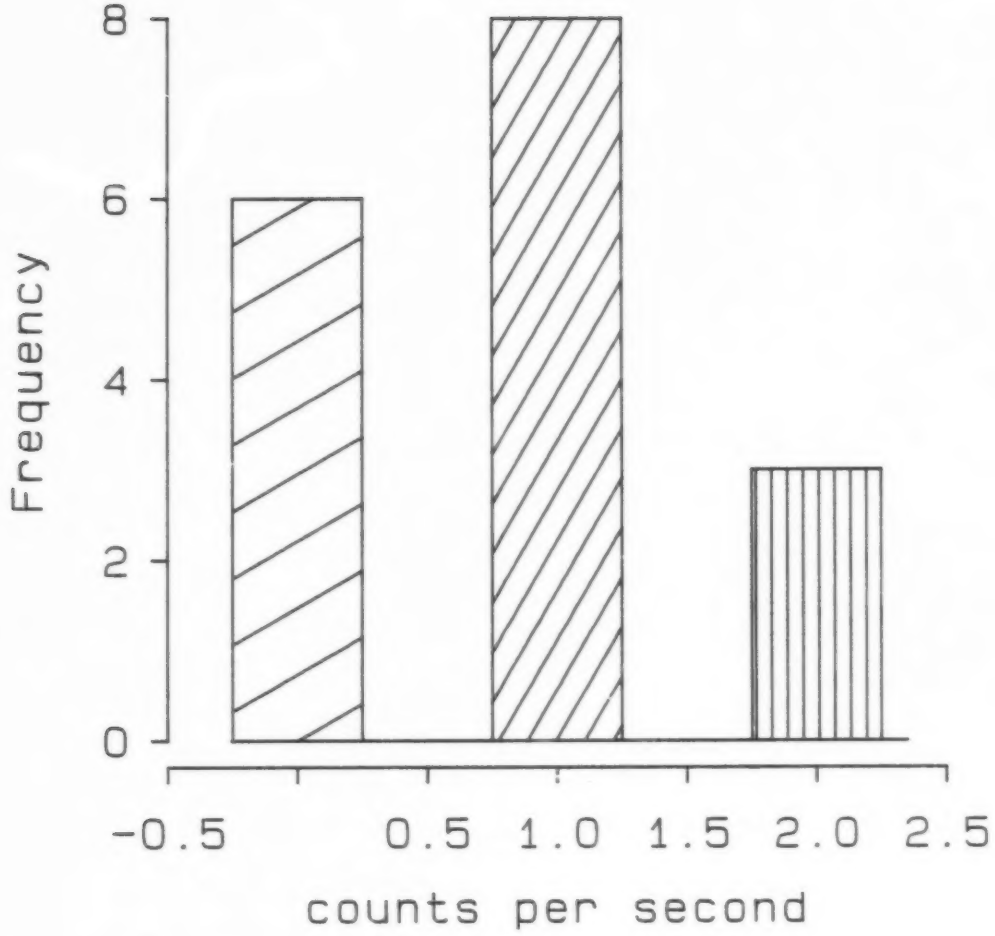

Fig. 28

A histogram of counts for the reference precordial signal for the first subject at rest. The low-frequency cut-off of the filter was increased from 500 to 850 Hz.

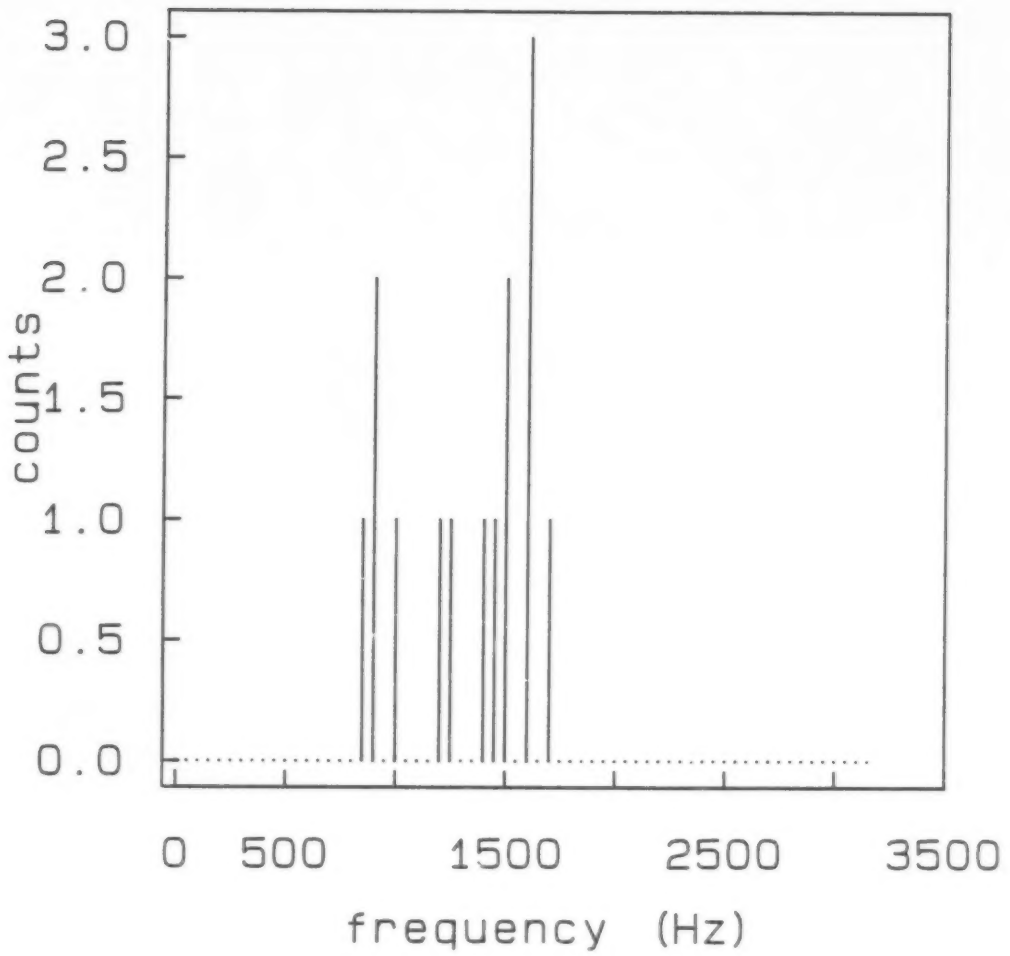

Fig. 29

A spectrogram showing the distribution of counts vs. frequency for the reference precordial signal of the first subject at rest, after the low-frequency cut-off of the filter was increased to 850 Hz.